Mineralogical Magazine (2021), **85**, 639–664
doi:10.1180/mgm.2021.72

CAMBRIDGE UNIVERSITY PRESS

Review Article

Mineralogy and mineral chemistry of quartz: A review

Jens Götze[1]*, Yuanming Pan[2] and Axel Müller[3,4]

[1] Institute of Mineralogy, TU Bergakademie Freiberg, Brennhausgasse 14, 09599 Freiberg, Germany; [2]Department of Geological Sciences, University of Saskatchewan, Saskatoon, Saskatchewan S7N 5E2, Canada; [3]Natural History Museum, University of Oslo, P.O. Box 1172, Blindern, 0318 Oslo, Norway; and [4]Natural History Museum, Cromwell Road, London SW7 5BD, UK

Abstract

Quartz (trigonal, low-temperature α-quartz) is the most important polymorph of the silica (SiO_2) group and one of the purest minerals in the Earth crust. The mineralogy and mineral chemistry of quartz are determined mainly by its defect structure. Certain point defects, dislocations and micro-inclusions can be incorporated into quartz during crystallisation under various thermodynamic conditions and by secondary processes such as alteration, irradiation, diagenesis or metamorphism. The resulting real structure is a fingerprint of the specific physicochemical environment of quartz formation and also determines the quality and applications of SiO_2 raw materials. Point defects in quartz can be related to imperfections associated with silicon or oxygen vacancies (intrinsic defects), to different types of displaced atoms, and/or to the incorporation of foreign ions in lattice sites and interstitial positions (extrinsic defects). Due to mismatch in charges and ionic radii only a limited number of ions can substitute for Si^{4+} in the crystal lattice or can be incorporated in interstitial positions. Therefore, most impurity elements in quartz are present at concentrations below 1 ppm. The structural incorporation in a regular Si^{4+} lattice site has been proven for Al^{3+}, Ga^{3+}, Fe^{3+}, B^{3+}, Ge^{4+}, Ti^{4+}, P^{5+} and H^{+}, of which Al^{3+} is by far the most common and typically the most abundant. Unambiguous detection and characterisation of defect structures in quartz are a technical challenge and can only be successfully realised by a combination of advanced analytical methods such as electron paramagnetic resonance (EPR) spectroscopy, cathodoluminescence (CL) microscopy and spectroscopy as well as spatially resolved trace-element analysis such as laser ablation inductively coupled plasma mass spectrometry (LA-ICP-MS) and secondary-ion mass spectrometry (SIMS). The present paper presents a review of the state-of-the-art knowledge concerning the mineralogy and mineral-chemistry of quartz and illustrates important geological implications of the properties of quartz.

Keywords: quartz, mineral chemistry, real structure, point defects, trace elements, electron paramagnetic resonance (EPR), cathodoluminescenece (CL)

(Received 25 June 2021; accepted 22 September 2021; Accepted Manuscript published online: 28 September 2021; Associate Editor: Martin Lee)

Introduction

The SiO_2 system is very complex. Though it has a simple chemical formula, SiO_2, at least 15 modifications or polymorphs are known, i.e. mineral phases with the same stoichiometric composition but different crystal structures. Quartz is the most important silica polymorph in nature, and occurs as a common constituent of magmatic, metamorphic and sedimentary rocks. In addition, quartz represents an economically important silica raw material. Both single crystals and polycrystalline quartz material are used in industry, for example, as high-purity quartz crystals or sands, refractory materials, or as an ore for silicon metal. For certain highly advanced applications, synthetic quartz crystals or SiO_2 materials are necessary due to increasing quality requirements not being easily met by silica raw materials (Götze and Möckel, 2012; Müller *et al.*, 2012, 2015).

The growing worldwide consumption of a wide range of high-technology applications means there is an increasing demand for high-quality natural quartz raw materials. Such high-purity quartz is defined as quartz containing less than 50 ppm of impurity elements, specifically < 30 ppm Al, < 10 ppm Ti, < 8 ppm Na and K, < 5 ppm Li and Ca, < 3 ppm Fe, < 2 ppm P and < 1 ppm B (Harben, 2002; Müller *et al.*, 2012). The type of impurities controlling the quality of high-purity quartz strongly influences the processing and potential use of the raw materials. Therefore, exploration for high-purity quartz deposits requires a thorough knowledge of the factors influencing the petrological and chemical properties of quartz. Several studies have shown that granitic pegmatites provide potentially the best sources of high-purity quartz (Larsen, 2000; Müller *et al.*, 2007, 2012, 2015).

The mineralogy and mineral chemistry of quartz are determined mainly by its defect structure. Certain point defects, dislocations, planar defects and micro-inclusions of fluids/melts and minerals can be incorporated into quartz during crystallisation under diverse thermodynamic conditions and by secondary processes, such as alteration, irradiation, diagenesis or metamorphism (Götze, 2009). The resulting real structure is not only a fingerprint of the specific physicochemical environment of quartz formation and secondary processes, but also determines the quality of SiO_2 raw materials. Therefore, quartz represents an important industrial raw material, and also serves as an important mineralogical and geochemical indicator for geological and ore-

*Author for correspondence: Jens Götze, Email: jens.goetze@mineral.tu-freiberg.de
Cite this article: Götze J., Pan Y. and Müller A. (2021) Mineralogy and mineral chemistry of quartz: A review. *Mineralogical Magazine* **85**, 639–664. https://doi.org/10.1180/mgm.2021.72

forming processes (e.g. Götze and Möckel, 2012 and references therein).

Quartz is one of the purest minerals, nevertheless minor impurities and defects have potentially significant importance and information, particularly regarding the mineral genesis. However, the detection and characterisation of such defects is generally a technical challenge and can only be successfully accomplished by a combination of advanced analytical methods, such as electron paramagnetic resonance (EPR) spectroscopy, cathodoluminescence (CL) microscopy and spectroscopy, synchrotron X-ray absorption spectroscopy (XAS) together with spatially resolved trace-element analysis such as laser ablation inductively coupled plasma mass spectrometry (LA-ICP-MS) and secondary-ion mass spectrometry (SIMS). Trace-element analysis provides general information about the types of impurities in quartz and their quantitative abundance. Information about the homogeneity or heterogeneity of quartz grains/crystals and the possible spatial distribution of defects can be obtained from CL measurements. Finally, EPR and XAS measurements yield additional information about the structural incorporation of trace elements and other structural defects not related to impurities, and are increasingly complemented by theoretical data from first-principles calculations. In addition, other spectroscopic techniques such as synchrotron XAS and Mössbauer spectroscopy, which have lower sensitivities than EPR techniques, have contributed useful information about the structural states of iron in quartz. In many cases, microscopic techniques (polarising microscopy, scanning electron microscopy (SEM), transmission electron microscopy (TEM), micro-Raman spectroscopy, or microbeam synchrotron X-ray fluorescence and XAS can complement the investigations.

This paper presents a review of the state-of-the-art knowledge concerning the mineralogy and mineral chemistry of quartz and the importance for better understanding of certain geological processes, together with improvements in technical processing of silica raw materials.

The mineralogy of quartz

Quartz is a mineral with the chemical formula SiO_2, which exists in two modifications in nature. The most common and most important modification is trigonal, low-temperature alpha-quartz, which is stable under surface conditions. At atmospheric pressure, alpha-quartz transforms at ca. 573°C into hexagonal, high-temperature beta-quartz. This transformation is reversible and is accompanied by a change of the density from 2.65 to 2.51 g/cm^3. The process also occurs, *vice versa*, during crystallisation from a melt or high-grade metamorphism during which the hexagonal high-temperature beta-quartz forms and subsequently transforms during cooling into the trigonal low-temperature modification. The structural changes during this transformation typically result in the formation of defects or twinning (Blankenburg *et al.*, 1994).

The crystal structure of alpha-quartz consists of a three-dimensional network of $[SiO_4]^{4-}$-tetrahedra, which are all linked via the oxygen atoms and are arranged in helical chains along the c-axis forming structural channels (Fig. 1). The left-handed or right-handed helices in the quartz structure correspond to morphologically right and left crystals, respectively (Donnay and Le Page, 1978; Glazer, 2018), which can be distinguished by the relative position of the trapezohedron face x to the positive main rhombohedron face r. The c-axis in the trigonal symmetry is identical with the optical axis and results in the optical uniaxial

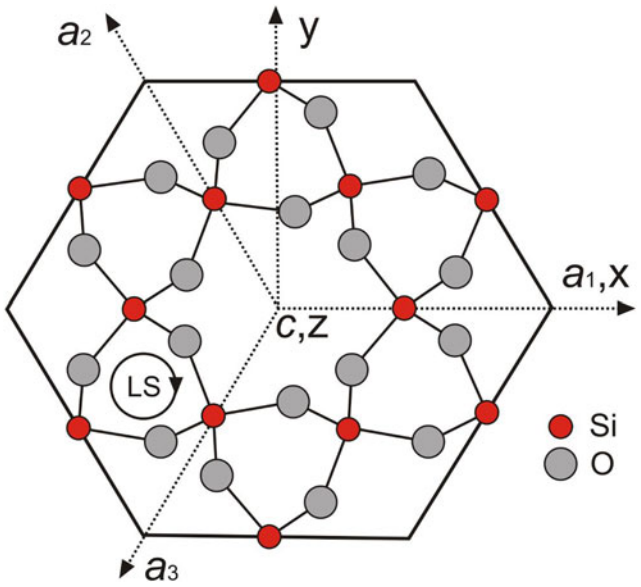

Fig. 1. Projection of morphologically right-handed α-quartz atomic positions onto the (0001) plane perpendicular to the c-axis, showing the EPR coordinate system (xyz), crystallographic axes a_1, a_2 and a_3, and z||c; the central c-axis large channel is seen to be surrounded by six c-axis small channels; LS denotes left-handed helices.

character of alpha-quartz. The silicon atom in the quartz structure resides on a two-fold axis, whereas all oxygen atoms are at general positions (Le Page *et al.*, 1980; Kihara, 1990; Baur, 2009). Each SiO_4 tetrahedron has two long and two short Si–O bonds at 1.613(2) Å and 1.603(2) Å, respectively, in quartz measured at 291 K and ambient pressure (Baur, 2009). Le Page *et al.* (1980) noted that the two Si–O bond distances are 1.611(1) Å and 1.606(1) Å at 94 K, and they do not change in the temperature range from 94 K to 298 K, however the Si–O–Si angle increases from 142.69(4)° to 143.65(5)°. In the EPR literature, the SiO_4 tetrahedron in the quartz structure is typically represented by the notation $[SiO_4]^0$ to emphasise its overall neutrality, whereas substitutional groups such as $[GeO_4]^0$ and $[AlO_4]^-$, together with their associated paramagnetic centres $[GeO_4]^-$ and $[AlO_4]^0$ are denoted accordingly (Weil, 1984; Mashkovtsev and Pan, 2013; Alessi *et al.*, 2014).

Several chemical and physical properties of quartz such as trace element and isotopic composition, luminescence behaviour, micro-inclusion inventory or colour are strongly dependent on the specific *P*–*T*–*x* conditions of its formation. These varying properties result in the development of numerous varieties, i.e. colour varieties such as amethyst, smoky quartz and rose quartz, or certain growth phenomena such as fibre and sceptre quartz, or microcrystalline quartz varieties such as chalcedony and quartzine (Rykart, 1995; Blankenburg *et al.*, 1994; Götze, 2009).

Point defects in quartz

Zero-dimensional point defects in quartz can be related to the incorporation of foreign ions in lattice sites and interstitial positions, to different types of displaced atoms, and/or to defects associated with silicon or oxygen vacancies (e.g. Weil, 1984, 1993; Stevens Kalceff, 2009; Nilges *et al.*, 2008, 2009; Pan *et al.*, 2009; Mashkovtsev and Pan, 2012a, 2012b; Mashkovtsev *et al.*, 2013a; Alessi *et al.*, 2014; Mashkovtsev and Pan, 2014). The latter represent pure lattice defects and can be generated without the

https://doi.org/10.1180/mgm.2021.72 Published online by Cambridge University Press

incorporation of impurity ions into the quartz lattice. Point defects can serve as the starting locations for more extended defects such as dislocations or planar defects (McLaren *et al.*, 1983, 1989; Lin *et al.*, 1994; McConnell *et al.*, 1995).

According to their electronic structure, point defects can be classified into diamagnetic and paramagnetic types and investigations are mainly recognised using EPR spectroscopy in combination with other spectroscopic methods (e.g. luminescence spectroscopy, UV-Vis-IR absorption spectroscopy, synchrotron XAS, Mössbauer spectroscopy) and trace-element analysis. Most of the paramagnetic centres in quartz are metastable, i.e. they are sensitive to irradiation and temperature treatment. However, some stable centres have also been detected, which can be formed by the incorporation of paramagnetic ions such as $H^{+/0}$, $Ag^{2+/0}$, Li^0, $Cu^{2+/0}$ or Ni^+, mainly in interstitial positions (Laman and Weil, 1977; Davis and Weil, 1978; Isoya *et al.*, 1983; Weil, 1993). Even these paramagnetic ions in quartz are mostly not intrinsic and are either incorporated by electron diffusion or converted from diamagnetic precursors via irradiation. Indeed, most point defects in quartz are diamagnetic, but can be converted to paramagnetic ones recognisable by EPR analysis, by various physical and chemical treatments (e.g. natural and artificial irradiation; Weil, 1984; Pan and Nilges, 2014).

The EPR techniques, with superior sensitivity unmatched by any other structural methods, have identified a large number of paramagnetic defects (and their diamagnetic precursors) in quartz (Supplementary Tables S1 and S2, see details below). In particular, the common detection and analysis of diagnostic hyperfine or superhyperfine structures of paramagnetic defects, which arise from interactions with non-zero-spin nuclei, not only aid in their unambiguous identification, but also typically provide definitive information about their geometric and electronic configurations. For example, ^{29}Si hyperfine structures, which is the only stable isotope of silicon with a non-zero nuclear spin (I = 1/2) and a natural isotope abundance of 4.7%, are often detected by EPR. However, analysis of ^{17}O hyperfine structures, which is the only stable isotope of oxygen with a non-zero nuclear spin (I = 5/2) and an exceedingly low abundance of 0.04%, generally requires artificially ^{17}O-enriched quartz samples (McEachern and Weil, 1994; Mashkovtsev *et al.*, 2013).

Aluminium

Aluminium is the prevailing impurity in quartz. The $[AlO_4]^0$ centre (Fig. 2) was first described in smoky quartz by Griffiths *et al.* (1954). This paramagnetic centre is the most common trace-element defect in quartz, which is caused by substitution of Si^{4+} by Al^{3+} with an electron hole localised at one of the four nearest O^{2-} ions. The precursor state for this paramagnetic centre is the diamagnetic $[AlO_4/M^+]^0$ defect with an adjacent charge compensating cation ($M^+ = H^+$, Li^+, Na^+) at an interstitial position in the c-axis channel (Botis *et al.*, 2009). These diamagnetic defects have been confirmed by the low-temperature EPR characterisation of the paramagnetic $[AlO_4/M^+]^+$ centres in quartz irradiated and measured at 77 K (Table S1; Mackey, 1963; Mackey *et al.*, 1970; Nuttall *et al.*, 1981a,b; Dickson and Weil, 1990; Walsby *et al.*, 2003; Botis and Pan, 2009, 2011). The paramagnetic $[AlO_4/M^+]^+$ centres are known to convert to the $[AlO_4]^0$ centre upon warming to room temperature (Cohen, 1956; Nuttall and Weil, 1981a; Walsby *et al.*, 2003). The optically active $[AlO_4]^0$ centre is responsible for the colour of smoky quartz (O'Brien, 1955; Meyer *et al.*, 1984). Nuttall and Weil (1981c) also reported the triplet-state (S = 1) centre $[AlO_4]^+$ in quartz measured at ~35 K after X-ray irradiation at 77 K (Table S1), which contains two electron holes, one at each of two symmetry-related oxygen atoms bonded to an aluminium substituting for silicon and apparently formed from the diamagnetic $[AlO_4/M^+]^0$ precursors as well.

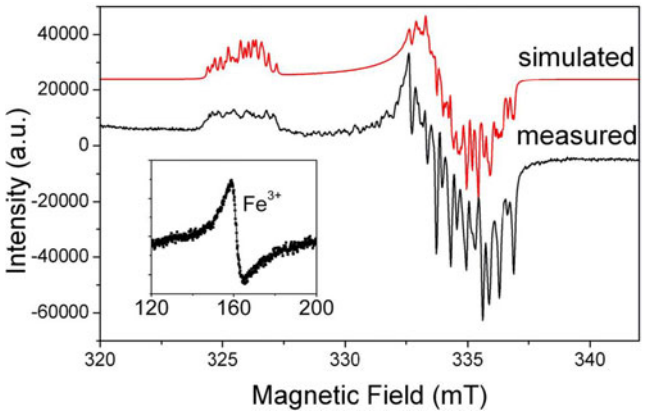

Fig. 2. Representative powder EPR spectrum of a high-purity quartz from Kyshtym (Russia) containing 4.2 ppm Al (Götze *et al.*, 2017) measured at a microwave frequency (ν) of ~9.39 GHz and temperature of 85 K, showing the $[AlO_4]^0$ centre. Also shown for comparison is the simulated spectrum of this centre using spin Hamiltonian parameters from Walsby *et al.* (2003). Insert is a room-temperature spectrum of the same sample containing <0.41 ppm Fe (i.e. the detection limit of LA-ICP-MS), showing a rhombic Fe^{3+} centre at the effective g = ~4.28.

Gemanium

Although the abundance of germanium in nature is low, the isovalent substitution of Ge^{4+} for Si^{4+} is common. The resulting diamagnetic $[GeO_4]^0$ defect in quartz can be transformed by ionising radiation at <100 K into two paramagnetic $[GeO_4]^-$ centres (Table S1), which are distinguished by the orbital of the unpaired spin lying along the different O–Ge–O bisectors of the GeO_4 tetrahedron (Mackey, 1963; Isoya *et al.*, 1978; McEachern *et al.*, 1992; McEachern and Weil, 1994). On warming above 150 K or irradiation at room temperature, the $[GeO_4]^-$ centres can capture M^+ ions (Li^+, Na^+ and Ag^+) released from associated $[AlO_4/M^+]^0$ centres and form the $[GeO_4/M^+]^0$ centres (Table S1; Mackey, 1963; Weil, 1971; Weil, 1984; Rakov *et al.*, 1985; Dickson *et al.*, 1991; McEachern *et al.*, 1992; McEachern and Weil, 1994; Claridge *et al.*, 2008).

In addition, multiply-compensated germanium electron centres such as $[GeHLi_2]$ and $[GeH^-H_1^+H_2^+]$ have been reported. They are interpreted to derive from the diamagnetic $[GeO_4/M_1M_2]$ precursors, containing a divalent Ge^{2+} ion and two monovalent charge compensators ($M = Li^+$, H^+, Na^+), by capturing a paramagnetic atomic hydrogen during irradiation (Weil, 1971; Laman and Weil, 1978; Weil, 1984).

Iron

Iron can be incorporated into quartz in three different valence states (Fe^{2+}, Fe^{3+} and Fe^{4+}; Cox, 1976, 1977; Cohen, 1985; Cressey *et al.*, 1993; Weil, 1994; Schofield *et al.*, 1995; Dedushenko *et al.*, 2004; Di Benedetto *et al.*, 2009; SivaRamaiah *et al.*, 2011; SivaRamaiah and Pan, 2012), in addition colloidal clusters of metallic iron have also been reported to occur in quartz (Daniels and Morton, 1981; SivaRamaiah and Pan, 2012). EPR

https://doi.org/10.1180/mgm.2021.72 Published online by Cambridge University Press

studies have established at least six distinct Fe^{3+} centres substituting for Si, as either the charge uncompensated $[FeO_4]^-$ centre or charge-compensated $[FeO_4/M^+]^0$ centres ($M^+ = Li^+$, H^+, Na^+, Table S1; Scala and Hutton, 1976; Mombourqette *et al.*, 1986, 1989; Halliburton *et al.*, 1989; Minge *et al.*, 1989, 1990; Weil, 1984, 1994). The larger ionic radius of Fe^{3+} (0.64 Å) compared to Si^{4+} (0.42 Å), means that the tetrahedra will be distorted. Therefore, the structural incorporation of Fe^{3+} is only possible in marginal parts of the quartz crystals or in fissures (Götze and Plötze, 1997). Higher amounts of iron can cause lattice defects promoting the formation of highly disordered areas such as in the case of amethyst (Mineeva *et al.*, 1991).

The $[FeO_4/M^+]^0$ centres can be converted to the $[FeO_4]^-$ centre by irradiation (Hutton and Troup, 1966; Stegger and Lehmann, 1989). This process also results in the conversion of Fe^{3+} to Fe^{4+} accompanied by the formation of the typical amethyst colour (Fig. 3; Lehmann and Moore, 1966; Stegger and Lehmann, 1989; Dedushenko *et al.*, 2004; Di Benedetto *et al.*, 2009). However, details concerning the Fe^{4+} site and its local environment have not been determined unequivocally (Cox, 1976, 1977; Dedushenko *et al.*, 2004; Di Benedetto *et al.*, 2009). Similarily, very little is known about the local structural environment of Fe^{2+} in quartz (Cressey *et al.*, 1993; Schofield *et al.*, 1995; Di Benedetto *et al.*, 2009), because the magnetic properties of Fe^{2+} with oxygen neighbours preclude its EPR observation at conventional X-band frequencies (Weil, 1994).

Titanium

Titanium is a typical trace impurity in quartz and isovalently substitutes as Ti^{4+} for Si^{4+} in the SiO_4 tetrahedra. The Ti^{4+} in the diamagnetic $[TiO_4]^0$ centre can be transformed to the paramagnetic $[TiO_4]^-$ centre during irradiation at low temperatures (Table S1; Bershov, 1970; Isoya and Weil, 1979; Weil, 1984; Bailey *et al.*, 1992; Bailey and Weil, 1992a,b). This $[TiO_4]^-$ centre is unstable above 120 K and, similar to the $[GeO_4]^-$ centres, can capture diffusing M^+ ions (H^+, Li^+, Na^+) to form charge compensated $[TiO_4/M^+]^0$ centres (Table S1; Wright *et al.*, 1963; Rinneberg and Weil, 1972; Weil, 1984; Matyash *et al.*, 1987; Isoya *et al.*, 1988; Bailey and Weil, 1991, 1992).

There is an ongoing discussion about the role of substitutional Ti as an origin for the rose colour in quartz (Wright *et al.*, 1963). Smith *et al.* (1978) suggested that the colour originates from a charge transfer between substitutional Ti^{4+} and interstitial Fe^{2+}. Investigations by Lehmann and Bambauer (1973) and Cohen and Makar (1985) showed that additional Ti^{3+} at interstitial structural channel sites is responsible for the rose colouration. However, further studies have shown that nano-inclusions of dumortierite can also produce the colour in massive rose quartz (Goreva *et al.*, 2001; Ma *et al.*, 2002).

Phosphorus

Phosphorus as a trace element has been shown to substitute for Si^{4+} in the quartz structure as EPR has detected several radiation-induced $[PO_4]^0$ centres (Table S1). In particular, Mashmeyer and Lehmann (1983) reported the $[O_3AlO^-PO_3]$ centre with a hole trapped on the bridging oxygen atom between substitutional Al and P atoms in quartz, providing unambiguous evidence for the coupled substitution: $P^{5+} + Al^{3+} = 2\ Si^{4+}$. In addition, Maschmeyer and Lehmann (1983) suggested that the $[O_3AlO^-PO_3]$ centre is responsible for radiation-induced rose colouration of quartz.

The aforementioned examples illustrate that there typically exists a close relation between point defects and the different colours of quartz (Lehmann, 1978; Rossman, 1994). Although several allochromatic colours in quartz such as green, blue and red are caused by micro-inclusions of impurities (e.g. dickite, rutile, hematite, goethite, celadonite and dumortierite), idiochromatic colours are mainly generated by chromophores (Rossman, 1994; Yang *et al.*, 2007; Scholz *et al.*, 2012). This group consists of ions of 3d elements (e.g. synthetic blue quartz: Co^{2+}, green chrysoprase: Ni^{2+}) or paramagnetic centres, which can be activated by irradiation (Lehmann, 1978; Meyer *et al.*, 1984). However, the discussion concerning the origin of colours in quartz is very complex and partly controversial and will not be made here in detail. A thorough review about the origin of colours in quartz is given by Rossman (1994).

A number of point defects can be attributed to oxygen and silicon vacancies or oxygen excess. Oxygen-excess centres in quartz include the peroxy linkage (≡Si–O–O–Si≡) and the peroxy radical (≡Si–O–O), an oxygen associated hole centre consisting of an O_2^- ion bound to a single silicon on three oxygen atoms (Friebele *et al.*, 1979). In addition, hydrogen excess from the H_2O crystallisation medium can also result in the formation of OH^- centres in quartz. This defect consists of a proton bound on a regular O^{2-} ion of the SiO_4 tetrahedron (Weil, 1984, 1993). In addition, the EPR detection of two H-trapped hole centres ($[H_4O_4]^+$ and $[H_3O_4]^0$) (Table S1) has been used to suggest the presence of the neutral diamagnetic precursor with four hydrogen atoms located at the tetrahedral Si site (i.e. the $[H_4O_4]^0$ or hydrogarnet defect; Nuttall and Weil, 1980; Lin *et al.*, 1994; Lees *et al.*, 2003; Jollands *et al.*, 2020). Similarly, the EPR detection of the $[HLi_2O_4]^0$) centre in gamma-ray-irradiated quartz suggests the presence of analogous diamagnetic precursors $[HLi_3O_4]^0$ or $[H_2Li_2O_4]^0$ (Table S1; Lees *et al.*, 2003).

The group of oxygen-vacancy electron centres

The group of oxygen-vacancy electron centres (OVEC) involves an oxygen vacancy (≡Si–Si≡) and can be divided into the E' and E'' types, denoting one and two unpaired electrons ($S = 1/2$ and 1), respectively (Table S2). The E' (the •Si≡O moiety) centres are the most frequent defects in quartz apart from Al centres and can occur in different stages depending on thermal stability and sensibility to irradiation (Griscom, 1985). The most common E'_1 centre can be formed by various irradiations involving alpha particles, electron beams, neutrons, gamma- and X-rays, and has been used as palaeo-dosimeters and geochronometers due to its high thermal stability (> 550°C) (Moiseev, 1985; Toyoda, 2011, 2016). In addition, the E'_1 centre in nature, induced by diverse radiation sources from U/Th-bearing rocks/fluids to potassic alteration, can be used as an indicator for the formation of uranium deposits when the dominant source of radiation is uranium (Pan *et al.*, 2006; Botis *et al.*, 2006, 2008; Cerin *et al.*, 2017). X-ray or fast-electron irradiation of Ge-doped quartz at room temperature yielded at least three Ge analogues of E' centres, including the Ge E'_1 centre stable up to 700 K, the Ge E'_2 centre with a hydrogen impurity stable up to 500 K, and another Ge(IV) centre unstable at room temperature (Fig. 4; Feigl and Anderson, 1970; Mashkovtsev *et al.*, 2013).

Understanding of the E'_1 and Ge E'_1 centres in quartz has evolved with increasingly complete EPR data and sophisticated

https://doi.org/10.1180/mgm.2021.72 Published online by Cambridge University Press

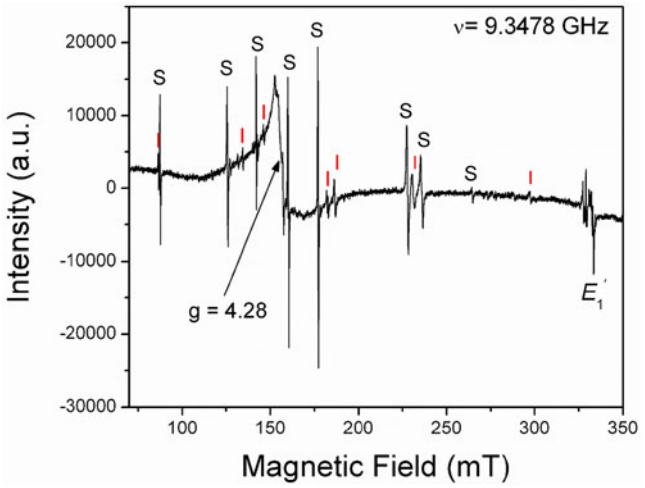

Fig. 3. Representative single-crystal EPR spectrum of a natural amethyst measured with B‖y and at 294 K. Letters S and I mark lines belonging to the S_1 ($[FeO_4/Li]^0$; Han and Choh, 1989; Halliburton *et al.*, 1989) and I centres, respectively. Note that the so-called interstitial (I) centre is actually $[FeO_4]^-$ with substitutional Fe ions at the Si sites (Mombouquette *et al.*, 1986). Also present are the broad signal at g = 4.28 and the E'_1 centre (modified from SivaRamaiah *et al.*, 2011).

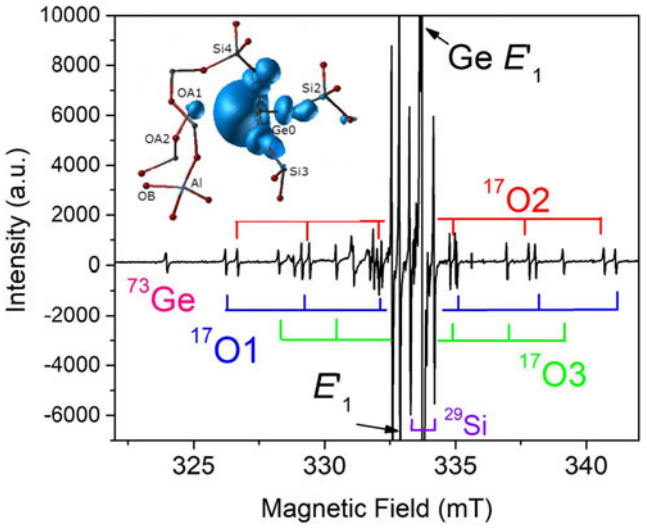

Fig. 4. Representative single-crystal EPR spectrum of an electron-irradiated, ^{17}O-enriched quartz (JC324) measured, after annealing at 573 K, with **B**‖c, room temperature and X-band frequency (~9.3 GHz; modified from Mahskovtsev *et al.*, 2013), showing three ^{17}O hyperfine sextets and one ^{73}Ge hyperfine line of the Ge E'_1 centre. Insert shows the 3D spin density of the Ge E'_1 centre calculated from the tri-vacancy with an Al impurity model.

first-principles calculations (Fig. 4; Li and Pan, 2012; Mashkovtsev *et al.*, 2013). The tri-vacancy model with an Al impurity, which best reproduces all available EPR data, involves the removal of one Si and two O atoms as well as the presence of a neighbouring Al impurity atom (Fig. 4; Li and Pan, 2012; Mashkovtsev *et al.*, 2013). Other well-characterised E' centres in quartz include the E'_4 and $E'_{11,16}$ centres (Table S2; Perlson and Weil, 2008; Mashkovtsev and Pan, 2012a, 2016, 2018; Mashkovtsev *et al.*, 2019). The former contains a proton near the oxygen vacancy, wheras the latter with diagnostic ^{27}Al superhyperfine structures provide experimental proof for the hypothesis that Al impurity plays an important role in the formation of E' centres (Jani *et al.*, 1983; Mashkovtsev and Pan, 2018; Mashkovtsev *et al.*, 2019). In addition, various E'' centres arising from interactions between two neighbouring E' centres have been discovered and characterised with the triplet-state model in recent years (Table S2; Mashkovtsev *et al.*, 2007; Mashkovtsev and Pan, 2011, 2012a, 2012b, 2014).

A family of silicon-vacancy hole centres is represented by different localisations of the unpaired electron on one, two or three oxygen atoms of the tetrahedra with silicon vacancies, which have been denoted as the O^-, O^{2-}, O_2^{3-} or O^{3-} type radicals (Fig. 5; Table S2; Mashkovtsev *et al.*, 1978; Botis *et al.*, 2005; Nilges *et al.*, 2008, 2009; Pan *et al.*, 2008, 2009; Mashkovtsev and Pan, 2013; Alessi *et al.*, 2014). By analogy to the notation for oxygen-vacancy electron centres, Mashkovtsev and Pan (2013) relabelled the silicon-vacancy hole centres as H'_1 to H'_7 (Table S2). The O^- centres with a hole trapped in a single nonbonding 2p orbital (i.e. the non-bridging oxygen hole centres or NBOHC; ≡Si–O) are very common defects in almost all quartz types, which can be detected by CL spectroscopy (Stevens Kalceff, 2009). However, the majority of the O^- centres in quartz are those associated with impurity ions such as Al^{3+} described above (Table S1) and are not linked with any silicon vacancy.

Several studies showed that defects associated with oxygen and silicon vacancies are most frequent in quartz crystallised at relatively low temperature (< 250°C) from amorphous silica precursors due to rapid cooling (Götze *et al.*, 1999, 2015a, 2020). Therefore, these defects are common in microcrystalline quartz

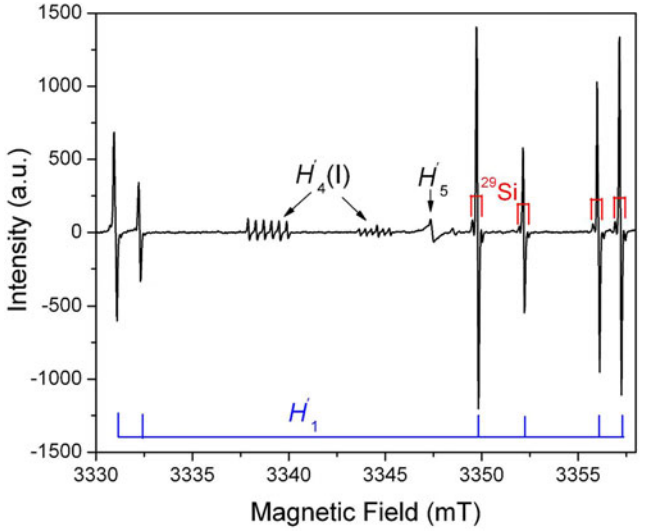

Fig. 5. Representative single-crystal EPR spectrum of an electron-irradiated quartz measured at W-band frequency (~94 GHz), B^c = ~140°, T = 110 K and a microwave power of 0.2 mW, illustrating three silicon-vacancy hole centres (H'_1, H'_4(I) and H'_5) (modified from Nilges *et al.*, 2009). Note that the H'_1 (alias #1) centre has six main lines corresponding to six magnetically inequivalent sites and that ^{29}Si hyperfine satellites are marked on four main lines. Also note that the two remaining main lines at ~3330 mT have irregular line shapes due to an incompletely resolved ^{27}Al superhyperfine structure (Nilges *et al.*, 2009). The H'_4(I) centre is characterised by a well-resolved ^{27}Al superhyperfine structure.

(agate, chalcedony) and in some hydrothermal quartz formed with high growth rates. In contrast, pegmatite quartz, in general, has a remarkably low abundance of defects associated with oxygen or silicon vacancies indicating growth of quartz from a parent melt/fluid under more or less constant physicochemical conditions (Götze *et al.*, 2004, 2005).

Moreover, partial dissolution experiments demonstrated that the silicon-vacancy hole centres in detrital quartz from the

https://doi.org/10.1180/mgm.2021.72 Published online by Cambridge University Press

Athabasca Basin (Canada) are concentrated preferentially along the grain margins. This observation is consistent with the limited penetration distances of alpha particles emitted from the decay of the uranium series present in palaeo-uranium-bearing fluids, providing the best linkage with mineralisation processes in uranium deposits (e.g. tracing the conduits of uranium-bearing fluids and constraining the sources of uranium; Pan *et al.*, 2006; Hu *et al.*, 2008; Cerin *et al.*, 2017).

In addition, abundant data exist on the health effects of quartz. This varies widely in emphasis from particle sizes/morphologies to surface properties and structural states. Long-term exposures to quartz and other silica forms (e.g. cristobalite and amorphous silica) are known to cause serious and potentially life-threatening diseases such as silicosis, fibrosis and lung cancer (Goldsmith, 1994). Of particular interest are the identification of various defects such as the peroxy and superoxide radicals and NBOHC on the surfaces of, and in, bulk quartz and their effects on toxicity and carcinogenic activity (Fubini *et al.*, 1990; Giordano *et al.*, 2007; Di Benedetto *et al.*, 2019, 2021). For example, Fubini *et al.* (1990) proposed the presence of these radicals on quartz surfaces or chemical functionalities as a possible mechanism for fibrogenecity via their reactions with macrophage oxygen metabolites, triggering the abnormal production of fibroblast stimulating factors and ultimately silicosis. However, a comprehensive synthesis of the voluminous literature on the health effects of quartz is beyond the scope of this review in which the emphasis is on geological contexts.

Cathodoluminescence properties of quartz

Cathodoluminescence (CL) is a powerful method, which enables the visualisation of the defect structure of minerals and reveals visually internal features caused by the varying spatial distribution of point defects that are not discernible by other analytical methods (Götze, 2012a; Götze *et al.*, 2013; Götze and Hanchar, 2018). In general, quartz and other SiO_2 modifications (including amorphous silica) show similar main luminescence emission bands. This is due to the fact that short-range order structural defects are caused mainly by silicon–oxygen and silicon–silicon interactions rather than by interactions between oxygen atoms (Walker, 1985). However, the band positions of the CL emissions can vary depending on the specific structure of the SiO_2 polymorph and experimental conditions (e.g. Walker, 1985; Luff and Townsend, 1990; Remond *et al.*, 1992).

The CL emissions for quartz are mostly weak but variable and the relation of specific luminescence emission bands to different defect centres causes a diversity of CL characteristics and visible CL colours, both in natural and synthetic quartz, depending on the processes of mineral formation or alteration (Table 1).

Therefore, knowledge about the origin of different luminescence centres can help to reconstruct geological processes and to reveal different growth generations (Fig. 6). However, the interpretation of the origin of CL emission bands in quartz is difficult due to a lack of stringent quantitative correlations between the intensities of CL bands and the concentrations of specific defects or trace elements.

In general, structural defects are much more important than trace elements as CL activators in quartz. Although correlations between CL zoning and several trace elements have been observed (e.g. Watt *et al.*, 1997; Müller *et al.*, 2003; Rusk *et al.*, 2006, 2008; Leeman *et al.*, 2012), the origin of the CL is related mostly to intrinsic lattice defects. The most common CL emission bands in natural quartz are bands with maxima at 450 and 650 nm (Ramseyer *et al.*, 1988; Götze *et al.*, 2001a). The visible luminescence colours of quartz in most igneous and metamorphic rocks and in some authigenic quartz depend on the relative intensities of these two dominant emission bands (Fig. 6).

Blue emission band at ~450 nm (2.75 eV)

The ~450 nm (2.75 eV) blue emission band (Fig. 6c) is related to oxygen deficiency centres (ODC) and is similar in amorphous and crystalline SiO_2 (Skuja, 1998). Recombination of the so-called self-trapped exciton (STE) involves an irradiation-induced electron hole pair (oxygen Frenkel pair) consisting of an oxygen vacancy and a peroxy linkage (Stevens Kalceff and Phillips, 1995). The blue emission at ca. 450 nm is probably the most common CL emission in natural quartz and can be detected in almost all quartz types.

In addition to the evidenced activation of the 450 nm band by a structural defect, several studies reported a strong correlation between the intensity of luminescence and the concentration of Ti in quartz, with the brightest CL corresponding to the highest Ti concentrations (e.g. Müller *et al.*, 2002, 2003; Van den Kerkhof *et al.*, 2004; Rusk *et al.*, 2008; Leeman *et al.*, 2012; Drivenes *et al.*, 2016). Up to now there has been no serious spectroscopic evidence that Ti is responsible for the activation of the blue emission in quartz. However, recent systematic studies of Ti-rich natural quartz from igneous rocks, as well as synthetic quartz from Ti-diffusion experiments could prove that Ti might also be responsible for the activation of the 450 nm luminescence emission band (unpublished data – compare with Fig. 22).

Red emission band at 620–650 nm

The red emission band at 620–650 nm (1.95–1.9 eV; Fig. 6c) is attributed to the recombination of electrons in the non-bridging oxygen band-gap state with holes in the valence-band edge (Siegel and Marrone, 1981; Stevens-Kalceff, 2009). A number of different precursors of this NBOHC has been proposed such as strained silicon–oxygen bonds, hydrogen or sodium impurities, or peroxy linkages (Stevens-Kalceff and Phillips, 1995). The formation of the NBOHC from these different defects causes variations of the band position. It is assumed that the 620 nm (1.95 eV) component is characteristic for hydroxyl precursors (:Si–OH), which are common in hydrothermal and authigenic quartz as well as silicified wood (Stevens-Kalceff *et al.*, 2000).

The CL emission at 1.9 eV (650 nm) commonly increases during electron irradiation due to the formation of NBOHC from different precursors. A high state of lattice damage can be attained in radiation-damaged quartz. The creation of NBOHC defects by bond breaking due to the α-particles was observed in both natural radiation-damaged quartz samples and in radiation experiments (e.g. Komuro *et al.*, 2002; Krickl *et al.*, 2008). In natural quartz, such lattice damage causes halos around U- and Th-bearing accessory minerals or migration tracks of U-bearing fluids (Fig. 7), which cannot be detected by conventional microscopic techniques (e.g. Owen, 1988; Ramseyer *et al.*, 1988; Meunier *et al.*, 1990; Götze *et al.*, 2001a ; Botis *et al.*, 2005; Cerin *et al.*, 2017).

Yellow emission band at 570 nm (2.15 eV)

Another defect-related CL emission in quartz is a broad yellow emission band centred at 570 nm (2.15 eV) that was first observed

https://doi.org/10.1180/mgm.2021.72 Published online by Cambridge University Press

Table 1. Main emission bands in CL spectra of quartz and suggested activators (modified after Götze, 2012a).

Emission	Suggested activator	References
175 nm (7.3 eV)	Intrinsic emission of pure SiO_2	Entzian and Ahlgrimm (1983)
290 nm (4.28 eV)	Oxygen vacancy	Jones and Embree (1976); Stevens-Kalceff (2009)
330–340 nm (3.75–3.6 eV)	Oxygen vacancy	Rink *et al.* (1993)
	$[AlO_4/Li^+]$ centre	Demars *et al.* (1996)
	$[TiO_4/Li^+]$ centre	Plötze and Wolf (1996)
380–390 nm (3.2–3.1 eV)	$[AlO_4/M^+]$ centre; $M^+ = Li^+$, Na^+, H^+	Alonso *et al.* (1983)
	$[H_3O_4]^0$ hole centre	Gorton *et al.* (1996); Yang and McKeever (1990)
450–460 nm (2.8–2.7 eV)	ODC / E'_1 centre with self-trapped exciton (STE)	Stevens-Kalceff and Phillips (1995)
	Substitutional Ti	Stevens-Kalceff (2009)
500 nm (2.45 eV)	Interstitial impurity cations	Ramseyer and Mullis (1990)
	(Li^+, Na^+, H^+)	Perny *et al.* (1992); Götze *et al.* (2005)
500–600 nm (2.45–2.06 eV)	Uranyl ion (UO_2^{2+})	Gorobets and Rogozine (2002)
Multiple lines		Götze *et al.* (2015a)
570 nm (2.15 eV)	Self-trapped exciton (STE) (strong disorder and oxygen deficiency)	Götze *et al.* (2015b)
620–650 nm (1.95–1.9 eV)	Non-bridging oxygen hole centre (NBOHC) with several precursors	Siegel and Marrone (1981); Stevens-Kalceff and Phillips (1995)
705 nm (1.65 eV)	Substitutional Fe^{3+}	Pott and McNicol (1971); Gorobets and Rogozine (2002)
1280 nm (0.97 eV)	Interstitial molecular oxygen	Stevens-Kalceff (2009)

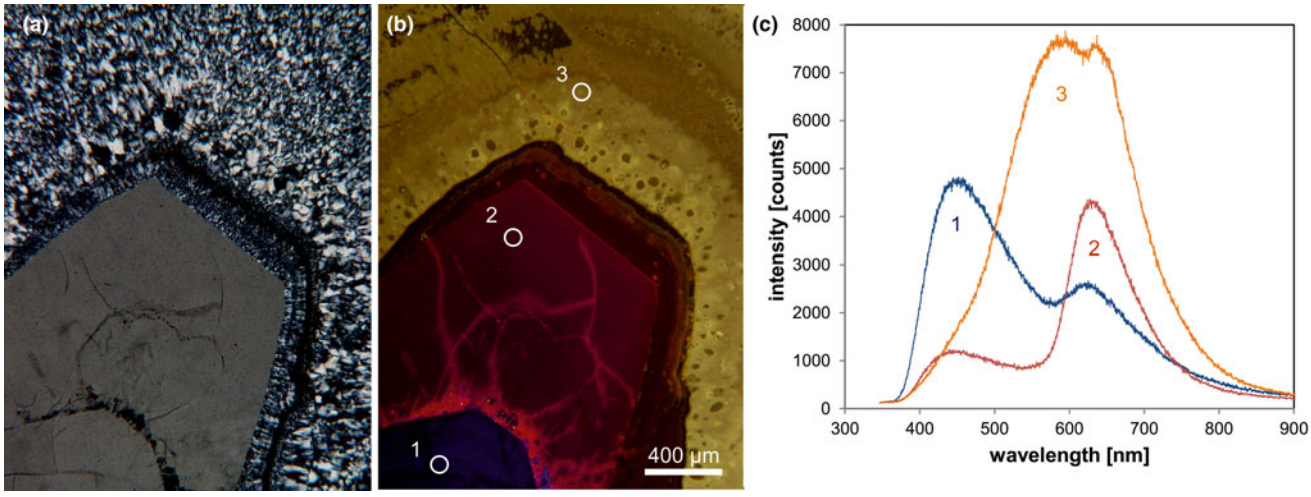

Fig. 6. Photomicrographs of quartz in transmitted light (crossed polars – a) and CL (b) in a rhyolite from Kemmlitz (Saxony, Germany); different quartz generations are distinguishable by different CL colours: (1) primary quartz phenocryst with blue CL, (2) reddish volcanic quartz of a second generation, (3) secondary microcrystalline quartz of hydrothermal origin with yellow CL. (c) The volcanic quartz exhibits two main emission bands at 450 and 620 nm with varying intensity ratios, whereas the hydrothermal quartz has a main emission at 570 nm and a subordinate shoulder at 620 nm; the circles in (b) mark the positions of spectral CL analyses.

by Rink *et al.* (1993) in natural quartz of hydrothermal origin and Götze *et al.* (1999) in agates of acidic volcanic rocks and hydrothermal vein quartz (Fig. 6c). Götze *et al.* (2015b) showed that the appearance of the 570 nm emission band can be attributed to high oxygen deficiency and local structural disorder in quartz. The proposed luminescence centre model implies self-trapped exciton (STE) emissions from strongly disordered regions in quartz. Additional geochemical data proved that quartz with yellow CL occurs exclusively in a low-temperature hydrothermal environment (mostly <250°C) and is related to fast crystallisation in an environment with oxygen deficiency.

Blue emission band at 385 nm (3.15 eV)

Trace-element activated CL in quartz is rare, but can be observed for specific geological environments, in particular in hydrothermal and pegmatite quartz. A blue emission at the edge of the UV region with a maximum at ca. 385 nm (3.15 eV; Fig. 8) correlates well with the Al content and the concentration of paramagnetic $[AlO_4/M^+]$ centres (Alonso *et al.*, 1983; Luff and Townsend, 1990; Perny *et al.*, 1992). The short-lived blue CL is the typical feature of natural and synthetic hydrothermal quartz (Ramseyer *et al.*, 1988; Götze *et al.*, 2001a, 2009). Because of the sensitivity to electron irradiation, this emission has been attributed to the recombination of a hole trapped adjacent to a substitutional, charge-compensated aluminium-alkali ion centre (Stevens Kalceff and Phillips, 1995). The rapid attenuation of the 385 nm emission under an electron beam results from the dissociation and electromigration of the charge compensating cations out of the interaction volume under the influence of the irradiation induced electrical field (Perny *et al.*, 1992). However, Gorton *et al.* (1996) found a reduced 390 nm band even in ultrapure synthetic quartz and suggested that the 3.15 eV emission is probably not completely related to Al.

https://doi.org/10.1180/mgm.2021.72 Published online by Cambridge University Press

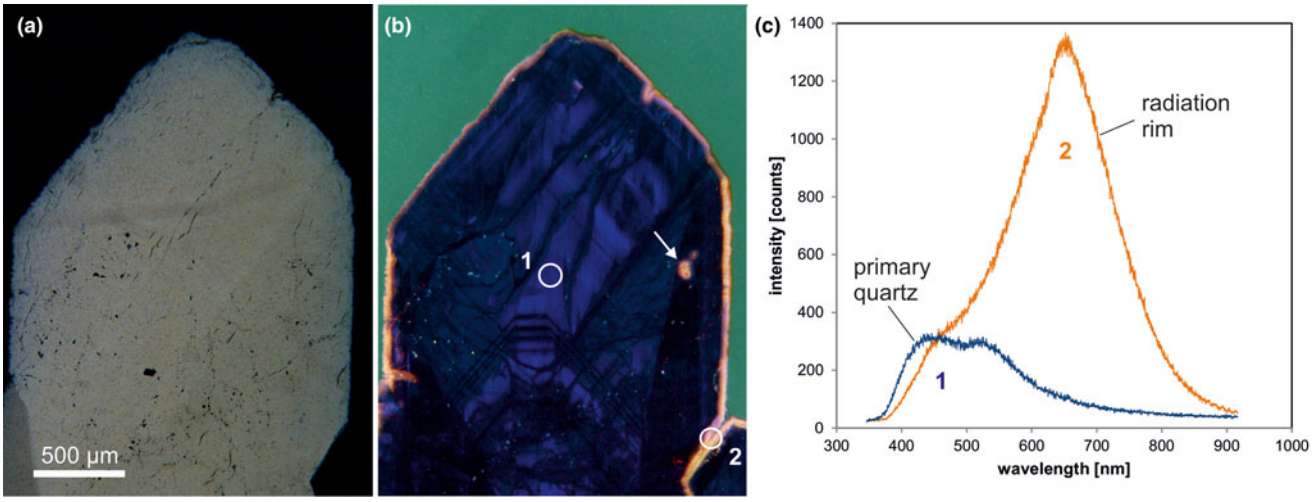

Fig. 7. Photomicrographs in transmitted light (crossed polars, a) and CL (b) of drusy quartz from the Arrow U-deposit, Athabasca basin (Saskatchewan, Canada); the CL image reveals a continuous yellow orange radiation rim around the crystal as well as radiation halos around radioactive inclusions (arrow). (c) The CL spectra display strong development of the 650 nm emission band (NBOHC) due to radiation induced lattice damage; the circles in (b) mark the positions of spectral CL analyses.

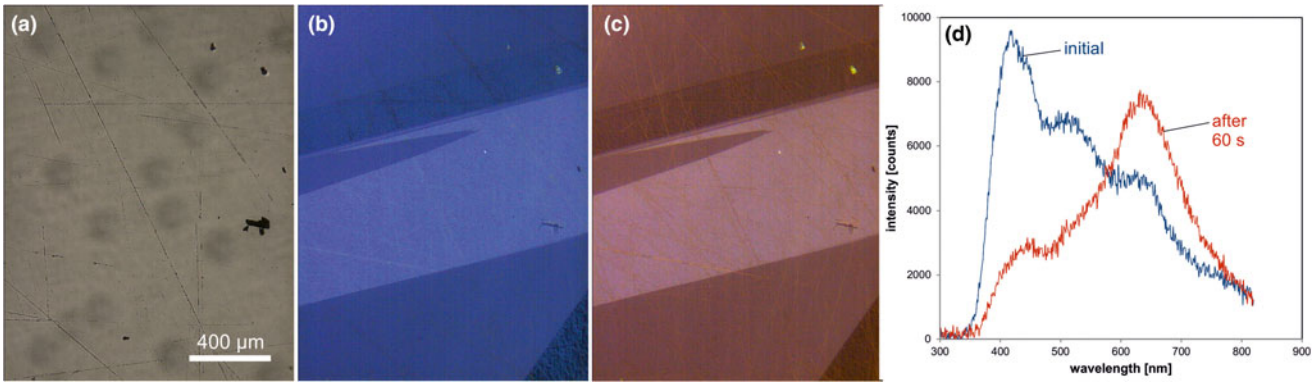

Fig. 8. Photomicrographs in transmitted light (crossed polars, a) and CL (b) of an Al-doped, synthetic hydrothermal quartz; CL reveals growth zones not visible in transmitted light. (c) The CL image after 60 s of electron irradiation reveals the transient character of the CL, which turns from initial blue (b) to reddish-brown (c). The related CL spectra (d) show a strong decrease of the blue emission band, whereas the red band increases due to the conversion of precursor centres (e.g. silanol groups :Si–OH) into the NBOHC.

Blue green emission at ~500 nm (2.45 eV),

Another trace-element related luminescence emission band in quartz is the short-lived blue-green CL (Fig. 9) at ca. 500 nm (2.45 eV), which can be related to the alkali-compensated trace-element centres in the quartz structure (Ramseyer and Mullis, 1990; Perny *et al.*, 1992, Götze *et al.*, 2005). Ramseyer and Mullis (1990) and Perny *et al.* (1992) performed CL measurements, microprobe analyses, temper and electro-diffusion experiments and concluded that the CL can be related to the uptake of positively charged interstitial cations (H^+, Na^+, Li^+) associated with the substitution of Al for Si. Several studies showed that the transient blue-green CL is a characteristic feature of pegmatite quartz and can also occur in hydrothermal and even in metamorphic quartz (Ramseyer and Mullis, 1990, Perny *et al.*, 1992; Götze *et al.*, 2001a, 2005; Sittner and Götze, 2018). Recent studies showed the predominance of Li^+ as a charge-balancing cation for the 500 nm CL emission in pegmatite quartz (Sittner, 2019).

The intensity of the blue-green CL falls off rapidly within 30 to 60 seconds during electron irradiation. This transient behaviour can be related to ionisation-enhanced diffusion of luminescence centres as was proved by electro-diffusion experiments (Ramseyer and Mullis, 1990). The short-lived CL can be restored by heating the quartz to 500°C for one day (Perny *et al.*, 1992) indicating an opposite mechanism to that of thermoluminescence. In contrast, gamma-irradiation causes a decrease in the intensity of the short-lived blue-green CL and an increase in smoky colouration (Ramseyer and Mullis, 1990). This can be explained by the conversion of $[AlO_4/M^+]^0$ luminescence centres into $[AlO_4]^0$ colour centres.

Green luminescence at ~500–600 nm

A remarkable feature of some microcrystalline silica varieties as well as macrocrystalline quartz in agates is greenish luminescence emitted in CL and under short-wave UV (<300 nm) excitation, which is uncommon in quartz of magmatic and metamorphic rocks (Fig. 10). There have also been a few reports about UV-excited green luminescence in opal and chert that have

https://doi.org/10.1180/mgm.2021.72 Published online by Cambridge University Press

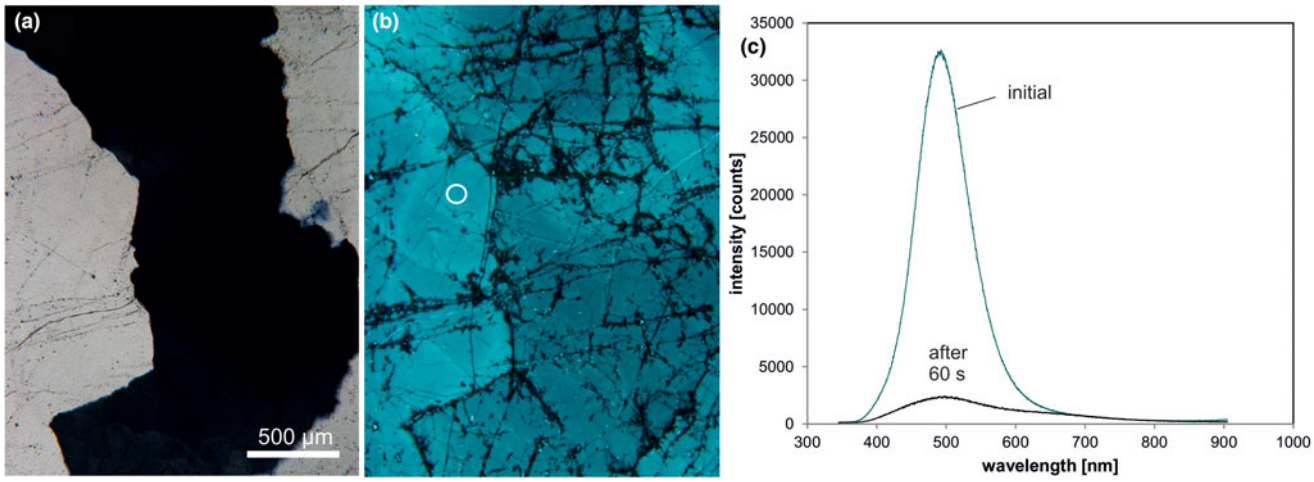

Fig. 9. Photomicrographs in transmitted light (crossed polars, a) and CL (b) of a pegmatite quartz from Heftetjern, Tørdal region (Norway); the sample exhibits the characteristic transient blue-green CL; fluid trails are visible due to dark CL. (c) The CL spectra show a drastic drop of the CL intensity of the 500 nm emission band during electron irradiation; the circle in (b) marks the position of spectral CL measurements.

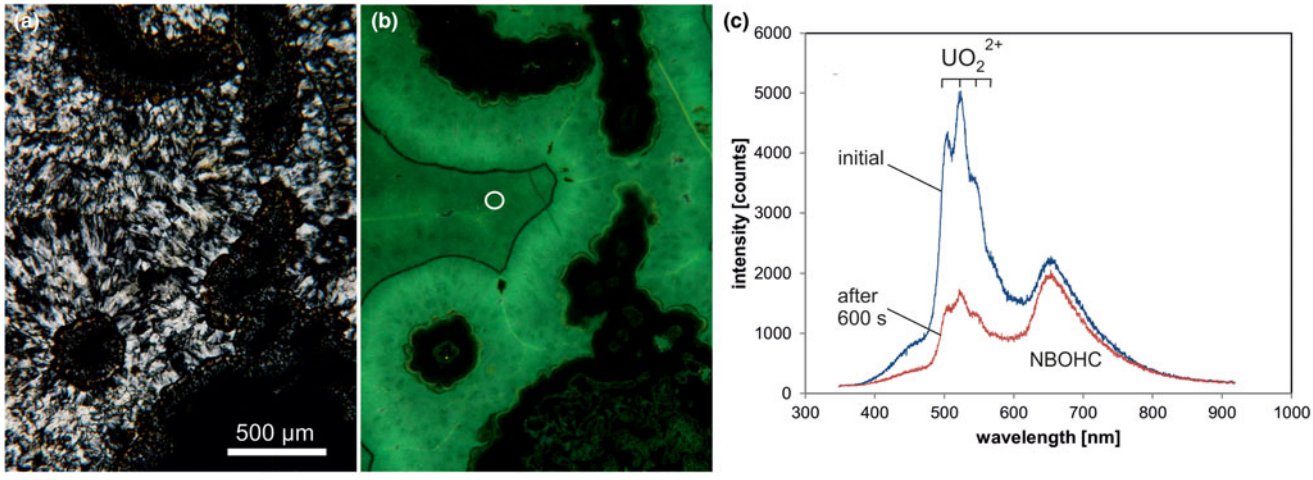

Fig. 10. Photomicrographs in transmitted light (crossed polars, a) and CL (b) of a chalcedony sample from Kardzali, Bulgaria; microcrystalline quartz exhibits a bright green CL. (c) The CL spectra reveal that uranyl (UO_2^{2+}) is responsible for the emission peak at ~500 nm accompanied by several equidistant lines; there is an additional CL emission band at 650 nm due to the non-bridging oxygen hole centre (NBOHC). The circle in (b) marks the position of spectral CL analyses.

elevated uranium concentrations (Gaillou *et al.*, 2008). The green luminescence is due to the electron transition from an excited to a ground state of the uranyl ion (UO_2^{2+}) and is shown by a typical emission line at ~500 nm (2.45 eV) accompanied by several equidistant lines (Götze *et al.*, 2015a; Fig. 10c). These are due to the harmonic vibrations of oxygen atoms along the uranyl axis (Gorobets and Rogojine, 2002). Recent studies have revealed that U is mainly incorporated in the form of a uranyl-silicate complex in opal and microcrystalline quartz (Pan *et al.*, 2021). The mechanism of the uranyl luminescence is very effective and can be detected in SiO_2 phases with U contents as low as 1 ppm.

Red luminescence at 705 nm (1.65 eV)

A CL emission band in the red on the edge to the infrared around 705 nm (1.65 eV) was first reported from synthetic quartz crystals (Pott and McNicol, 1971). It is assumed that this ~705 nm emission can be related to the substitutional incorporation of Fe^{3+} into the quartz lattice similar to other silicates such as feldspar minerals (Pott and McNicol, 1971; Gorobets and Rogojine, 2002). Some red luminescing quartz was also found in metasomatically overprinted granites from Khaldzan Buregte (Mongolia), where the ferric iron was probably mobilised during fenitisation processes (Kempe *et al.*, 1999). Because of the relatively large ionic radius of Fe^{3+} its incorporation into the quartz lattice is limited and therefore, the 705 nm emission is rare. Its origin has to be further verified by measurements of the luminescence lifetime and/or the luminescence excitation spectra.

Mineral chemistry of quartz

Quartz is one of the purest minerals in the Earth's crust in terms of chemical impurities expressed as trace-element contents. Due to limitations in charge and ionic radii only a limited number of ions can substitute for Si^{4+} in the crystal lattice or can be incorporated in interstitial positions. Therefore, most elements are

https://doi.org/10.1180/mgm.2021.72 Published online by Cambridge University Press

present in quartz in concentrations below 1 ppm (Müller *et al.*, 2003, 2012; Götze, 2009). The structural incorporation in a regular Si^{4+} lattice position has been proven for Al^{3+}, Ga^{3+}, Fe^{3+}, B^{3+}, Ge^{4+}, Ti^{4+} and P^{5+} (e.g. Weil, 1984), in which Al is probably the most common ion (up to a few 1000 ppm) because of its abundance in the Earth's crust and the similar ionic radii of Si^{4+} and Al^{3+}. Mono- and divalent ions, primarily H^+, Li^+, Na^+, K^+, Be^+, Rb^+ and Fe^{2+} may enter interstitial lattice positions in small amounts and charge-compensate trivalent substitutional ions, mainly Al^{3+} (Bambauer, 1961, Kats, 1962, Perny *et al.*, 1992, Stalder *et al.*, 2017, Potrafke *et al.*, 2019). For most other elements (e.g. Ca, Mg, Ba, Sr, REE, Mn, U and Th) capture by nano- (< 100 nm) or micro-inclusions (0.1–1 μm) of fluids or minerals is the most important mechanism (e.g. Gerler and Schnier, 1989; Müller *et al.*, 2003; Götze, 2009).

Aluminium

The structural incorporation of aluminium is evidenced by numerous studies using EPR spectroscopy (Alonso *et al.*, 1983). The substitution of Si^{4+} by Al^{3+} is mostly accompanied by charge compensating cations in interstitial positions. Combined studies by EPR, CL, spatially resolved trace-element analyses and SIMS mapping have revealed that Li^+ seems to be the dominant charge compensating ion in igneous and pegmatite quartz (Götze *et al.*, 2005; Beurlen *et al.*, 2011; Sittner, 2019), whereas H^+ plays an additional significant role in hydrothermal quartz and authigenic quartz in sedimentary/diagenetic environments (Bambauer, 1961; Miyoshi *et al.*, 2005; Müller and Koch-Müller, 2009; Jourdan *et al.*, 2009; Götte *et al.*, 2011; Lehmann *et al.*, 2011; Götte, 2016; Stalder *et al.*, 2017; Fig. 11). The preferred incorporation of H^+ in interstitial structural positions in natural and synthetic hydrothermal quartz can be explained by its input from the mineralising aqueous fluids (Bambauer *et al.*, 1962; Stenina, 2004). Further possible mechanisms of structural incorporation of Al^{3+} are the coupled substitution with a pentavalent ion or the charge compensation by electron defects on vacancies.

The concentration of Al in quartz in magmatic systems seems to be mainly controlled by the aluminium saturation index of the melt rather than by the temperature (Jacomon and Larsen, 2009; Breiter *et al.*, 2013, 2020). Accordingly, the Al concentration in quartz increases during melt evolution from metaluminous to peraluminous compositions. In hydrothermal systems, factors such as temperature, growth rate and Al concentration in the aqueous solution influence the Al content in quartz. It was shown that changes in pH have strong effects on Al solubility and the aqueous Al concentration, and thus cause variations of the Al concentration in hydrothermal quartz (e.g. Perny *et al.*, 1992; Rusk *et al.*, 2008; Müller *et al.*, 2010; Luo *et al.*, 2020).

The incorporation of Al into SiO_4 tetrahedra is limited by the ionic radius of the Al^{3+} ion (0.54 Å), which can occur both in fourfold and sixfold coordination with oxygen. Therefore, high amounts of Al substitution in quartz result in a distortion of the tetrahedra and destroy the perfection of the crystal lattice. Nevertheless, previous EPR studies of $[AlO_4]^0$ centres in chalcedony and the macrocrystalline quartz in agates have revealed abnormal high concentrations of structural Al in these SiO_2 phases (Götze *et al.*, 2001b). There are strong indications that the formation of some hydrothermal quartz and/or agate proceeds through several structural states of SiO_2 with amorphous silica as

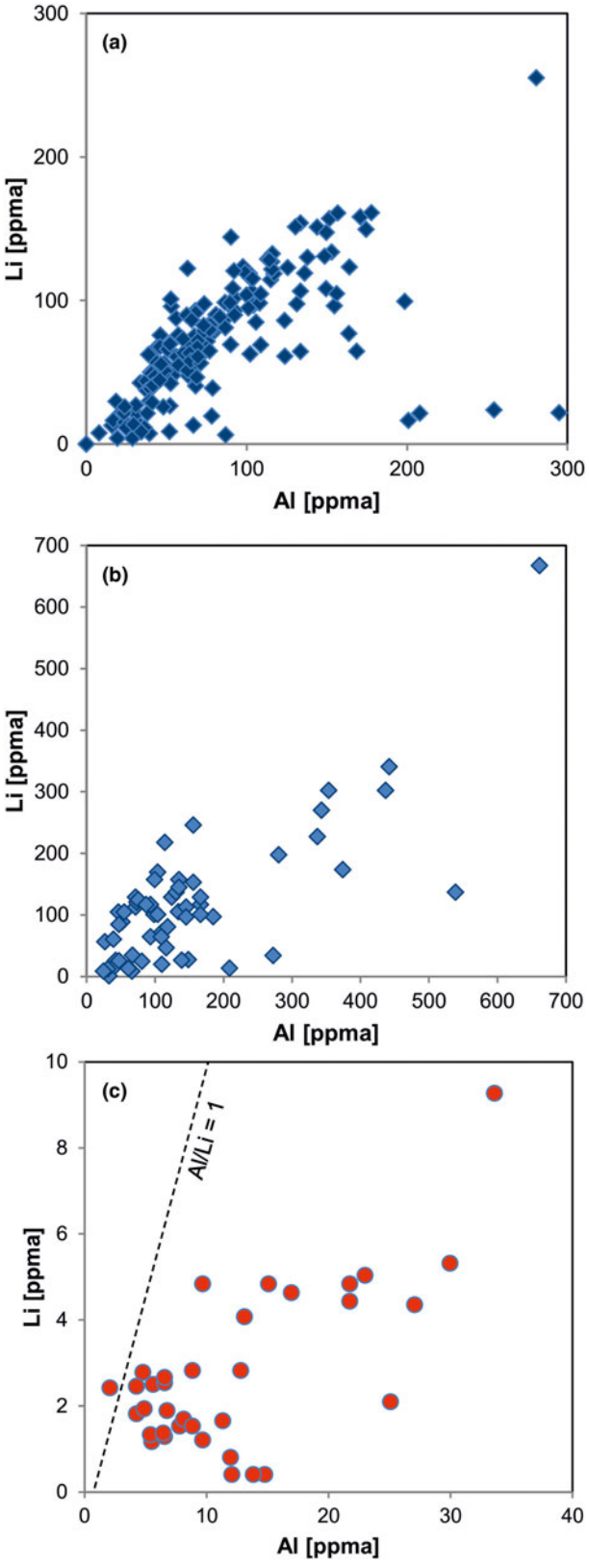

Fig. 11. Element correlation for Al *vs*. Li (ppma = atoms per 10^6 atoms Si) in quartz of different origin: (a) pegmatite quartz from Norway; (b) pegmatite quartz from different deposits in Norway and Namibia; (c) hydrothermal quartz from the Ural region, Russia. The pegmatite quartz shows almost 1:1 ratios of Al to Li, whereas the hydrothermal quartz is Li deficient (data from Götze *et al.*, 2004, 2017; Sittner, 2019).

https://doi.org/10.1180/mgm.2021.72 Published online by Cambridge University Press

the first solid phase (Dong *et al.*, 1995, Götze *et al.*, 2020). This might result in areas or zones with a high degree of disorder and large numbers of lattice defects (oxygen and silicon vacancies), which enable the incorporation of high concentrations of 'defect' Al. Such a scenario could also explain the extreme high concentrations of Al in neighbouring individual growth zones or generations of hydrothermal quartz, which reflect abrupt changes in the physicochemical conditions (open hydrothermal system).

Titanium

In contrast to Al, titanium can be both incorporated as substitutional ion for Si^{4+} and bound on mineral micro-inclusions such as rutile or anatase. The geochemical compatibility of Ti and its relatively large ionic radius (Ti^{4+} 0.61 Å) results in a preferred uptake in early formed quartz at high temperatures and pressures. Therefore, the highest Ti contents in quartz can be found in quartz phenocrysts in volcanic rocks and early crystallised quartz grains in igneous rocks. In granitic melts, decrease in the Ti concentrations in quartz can be observed during increasing fractionation and decreasing temperature (Larsen *et al.*, 2004; Breiter and Müller, 2009). The lowest Ti concentrations in quartz were measured in quartz crystallised from aqueous solutions at relatively low temperatures (Blankenburg *et al.*, 1994; Müller *et al.*, 2003). Using the temperature dependence of Ti uptake in quartz, Wark and Watson (2006) created a Ti-in-quartz geothermometer based on the Ti concentration in quartz. Subsequently, Huang and Audétat (2012) discovered, in addition, that Ti incorporation in quartz is slightly controlled by the crystallisation pressure, and modified the geothermometer to a Ti-in-quartz geothermobarometer. The geothermobarometer is, however, very sensitive to the Ti saturation of the melt in which the quartz crystallises and thus has to be applied with caution.

The limitations in structural compatibility of Ti frequently cause exsolution phenomena at lower temperatures, such as the formation of TiO_2 micro-inclusions (rutile, anatase) in quartz crystals. Ti^{4+} is commonly sixfold coordinated by oxygen because of its ionic radius. The substitution of fourfold coordinated Ti^{4+} for Si^{4+} in the tetrahedral position is only possible at elevated temperatures. Therefore, a straight correlation between bulk Ti contents in quartz and structural Ti measured by EPR spectroscopy is often missing (Fig. 12). However, it should also be considered that Ti can be incorporated as a diamagnetic $[TiO_4]^0$ centre that cannot be detected by EPR spectroscopy.

Germanium

Germanium shows a similar geochemical behaviour compared to Si, in addition Ge^{4+} has a similar ionic radius (0.53 Å). Therefore, Ge^{4+} can substitute isovalently for Si^{4+} in the SiO_4 tetrahedra. However, Ge belongs to the group of elements occurring in low concentrations in the Earth's crust (Clark value 1.4 ppm) mostly resulting in low concentrations in quartz. Germanium does not partition into any particular mineral phase and is therefore enriched in residual melts or fluids. In particular the presence of halogens (e.g. fluorides) in the crystallisation medium favours the development of durable and volatile compounds (Walenczak, 1969). Thermodynamic considerations suggest that the transport and accumulation of Ge as the GeF_4 complex during chemical transport reactions could probably explain elevated Ge concentrations in quartz in specific geological environments (Götze *et al.*, 2012).

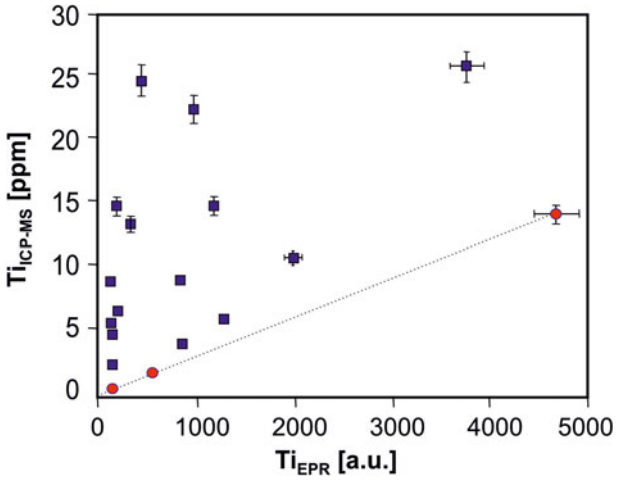

Fig. 12. Plot of Ti content in quartz measured by ICP-MS *vs.* concentration of structural Ti ($[TiO_4/Li^+]^0$ centres) determined by EPR spectroscopy (concentrations were determined as peak to base intensity under constant analytical settings according to Moiseev, 1985). Pegmatite quartz samples from the Rubicon Mine, Namibia (red circles) exhibit a linear correlation with zero intercept indicating a complete presence of Ti as structural substituent for Si; quartz samples from Norway (blue squares) are mostly far away from the correlation and show higher Ti contents; in these samples micro-inclusions of rutile were detected (data from Götze *et al.*, 2004).

Germanium contents in quartz from magmatic and metamorphic rocks are mostly in the range between 0.5 and 1.5 ppm (Walenczak, 1969; Blankenburg *et al.*, 1994). In most hydrothermal quartz, the Ge content is similar. Only some hydrothermal quartz veins in paragenesis with metalliferous deposits show elevated Ge contents up to several ppm (Blankenburg *et al.*, 1994; Müller *et al.*, 2018; Breiter *et al.*, 2020). Concentrations of >1.5 ppm up to 23 ppm Ge were measured in quartz crystallised from fractionated granitic and pegmatitic magmas (Götze *et al.*, 2004; Beurlen *et al.*, 2011; Breiter *et al.*, 2014). Extraordinary Ge concentrations of partially > 90 ppm were found in micro- and macrocrystalline quartz of agates, which exceeded the average concentration of the Earth's crust and also the Ge content in the surrounding host rocks (Götze *et al.*, 2016, 2020).

Phosphorus

Phosphorus can substitute as P^{5+} with an ionic radius of 0.38 Å for Si^{4+} in the quartz structure. A coupled mechanism $2\ Si^{4+} \leftrightarrow P^{5+} + M^{3+}$ ($M^{3+} = Al^{3+}$, B^{3+}) is assumed for the structural incorporation with Al^{3+} as the most frequent charge compensator, confirmed by the paramagnetic $[O_3AlOPO_3]^+$ centre (Maschmeyer and Lehmann, 1983). However, P is generally not considered in analytical measurements. Therefore, a specified procedure for the precise determination of P in quartz was developed by Müller *et al.* (2008).

The absolute concentration of P in quartz is mostly low and rarely exceeds several ppm (e.g. Larsen *et al.*, 2004; Müller *et al.*, 2003, 2012; Beurlen, 2011; Breiter *et al.*, 2013, 2020; Sittner, 2019). The concentration of P is typically buffered by the presence of fractionating mineral phases that particularly incorporate it at the expense of the residual melt and quartz. Therefore its distribution in quartz seems to be erratic (Beurlen *et al.*, 2011). Nevertheless, it seems to be slightly enriched during the differentiation of granitic and pegmatitic systems in late crystallisation phases (Larsen *et al.*, 2004).

https://doi.org/10.1180/mgm.2021.72 Published online by Cambridge University Press

Iron

Iron can be incorporated structurally by substituting for Si^{4+} in the tetrahedra or in interstitial sites. However, the ionic radii of Fe^{2+} (0.78 Å) and Fe^{3+} (0.65 Å) are much larger than that of Si^{4+}. Therefore, the incorporation is limited and mostly occurs in marginal parts or damaged areas of quartz crystals (Mineeva *et al.*, 1991; Götze and Plötze, 1997). Therefore, elevated contents of Fe in quartz can mostly be related to micro-inclusions of Fe-bearing minerals (e.g. hematite, goethite) or nano-clusters of amorphous Fe-compounds.

Boron

Boron mostly occurs in low concentrations (< 1 ppm) in quartz (Blankenburg *et al.*, 1994). Elevated contents of > 10 ppm B have been measured in quartz of pegmatites (e.g. Götze *et al.*, 2004; Beurlen *et al.*, 2011; Müller *et al.*, 2012), and remarkably high concentrations of up to 46 ppm were detected in quartz of agates from different locations (Götze *et al.*, 2020). Similar to Ge, a preferred transport of boron as a volatile BF_3 complex during chemical transport reactions could be responsible for the accumulation of B in quartz, if halogens were available in the participating fluids (Götze *et al.*, 2012).

The existence of nano-inclusions of tourmaline has been discussed as a possible reason for high B contents in pegmatite quartz (Müller *et al.*, 2012). However, quartz commonly lacks such impurities and a structural incorporation of boron must be assumed by analogy with other silicates (Grew and Hinthorne, 1983). Because of the small ionic radius of the B^{3+} ion (0.27 Å), the formation of planar BO_3-groups in minerals is commonly favoured (Jolland *et al.*, 2020), however the incorporation as BO_4 tetrahedra is also possible. Therefore, a coupled substitution of B^{3+} with pentavalent ions (P^{5+}) in two neighbouring MO_4 tetrahedra or in combination with charge-balancing cations and electron defects, respectively, has to be considered.

Gallium

Gallium occurs at very low concentrations in natural quartz (< 0.1 ppm) and is, thus, rarely detected. Walenczak (1969) was probably the first who reported Ga concentrations of igneous, metamorphic and hydrothermal quartz. In most of the quartz investigated, Ga showed concentrations between 0.02 and 0.4 ppm and amethyst had generally high Ga up to 25 ppm. Recent publications, applying *in situ* micro-beam techniques with very low detection limits for trace-element determination, have not confirmed such high Ga contents in natural quartz, and only chalcedony and macrocrystalline quartz of agates had Ga contents of 1–2 ppm (Götze *et al.*, 2015a). Müller *et al.* (2021) has shown, however that Al and Ga concentrations in quartz correlate (Fig. 13).

Alkali and alkali earth elements

Alkali and alkali earth elements can occur in elevated concentrations (up to >100 ppm) in quartz. In principle, cations such as Li^+, Na^+ or K^+ can be incorporated in interstitial positions (Botis *et al.*, 2009), where Li^+ is the most common charge-compensating ion. The lithophile character of Li probably favours its partition into silicate melts and quartz rather than in aqueous fluids. Therefore, it prefers the incorporation into structural channels for the charge compensation of Al rather than the concentration in fluid inclusions (Götze *et al.*, 2004). Hence, the uptake of Li in the quartz lattice seems to be mostly limited by the amount of substitutional Al (Müller and Koch-Müller, 2003). The availability of Li at time of quartz crystallization is thereby also controlled by the crystallization order of Li minerals and quartz in granites and granitic pegmatites.

Although Na and K were also proven to be potential charge compensators (e.g. Heaney and Davis, 1995; Botis *et al.*, 2009; Luo *et al.*, 2020), these ions are more commonly hosted by micro-inclusions of minerals and fluids or accumulated along micro-fissures (e.g. Günther *et al.*, 1998, Müller *et al.*, 2003; Götze *et al.*, 2004, 2017; Sittner, 2019; Ladenburger *et al.*, 2020). For instance, K is commonly associated with Al in quartz of granitic igneous rocks and pegmatites as nano-inclusions of K-feldspar or sheet silicates (e.g. Zolensky *et al.*, 1988; Jacamon, 2006; Jacamon and Larsen, 2009; Seifert *et al.*, 2011). Müller *et al.* (2012), for instance, suggested a formation of micro-inclusions with muscovite composition due to accumulation of Al and K during deformation processes. However, the majority of K, Na, Rb, Cs, Ca, Mg and Sr seems to be bound preferentially to fluid inclusions.

In general, the trace amounts of most alkali and alkali earth elements in quartz show parallel trends because of their similar geochemical behaviour (Figs 14, 15). The data indicate that the majority of elements is bound preferentially to micro-inclusions. Chemical investigations of inclusion fluids in quartz revealed that those inclusions play a major role in hosting alkali and alkali earth elements (e.g. Rossman *et al.*, 1987; Gerler, 1990; Gerler and Schnier, 1998; Günther *et al.*, 1998; Götze *et al.*, 2004; Ladenburger *et al.*, 2020). For instance, Bottrell *et al.* (1988) reported evidence for the presence of Na, K, Mg and Ca in fluid inclusions of different quartz samples.

Rare earth elements

Rare earth elements (REE) generally have very low concentrations in quartz. Therefore, their absolute abundance is not typically determined. However, REE distribution patterns are commonly used for the reconstruction of mineral forming processes and thus, the distribution of REE in quartz can provide useful information about the geological environment of quartz formation (Monecke *et al.*, 2000, 2002; compare with Fig. 20).

Because of their crystal-chemical properties, REE cannot be incorporated into the quartz crystal structure. It is assumed that REE in quartz are hosted preferentially in fluid inclusions. Rossman *et al.* (1987), Ghazi *et al.* (1993) and McCandless *et al.* (1997) reported a correlation of REE together with Rb and Sr with fluid-inclusion water indicating that these elements are mostly contained in the inclusion fluids. These results were confirmed by Götze *et al.* (2004) for pegmatite quartz, who found a correlation of REE contents in quartz with the absolute amount of inclusion fluid (Fig. 16). On the basis of these considerations, REE may provide important fingerprints concerning the composition of mineral forming fluids.

Antimony

Antimony is another trace element in quartz that can probably be related to a supply by mineralising fluids. Although the concentration of Sb in most quartz of igneous, volcanic and metamorphic rocks is far below 1 ppm (Blankenburg *et al.*, 1994), Rusk *et al.* (2011) found detectable Sb contents in quartz of

https://doi.org/10.1180/mgm.2021.72 Published online by Cambridge University Press

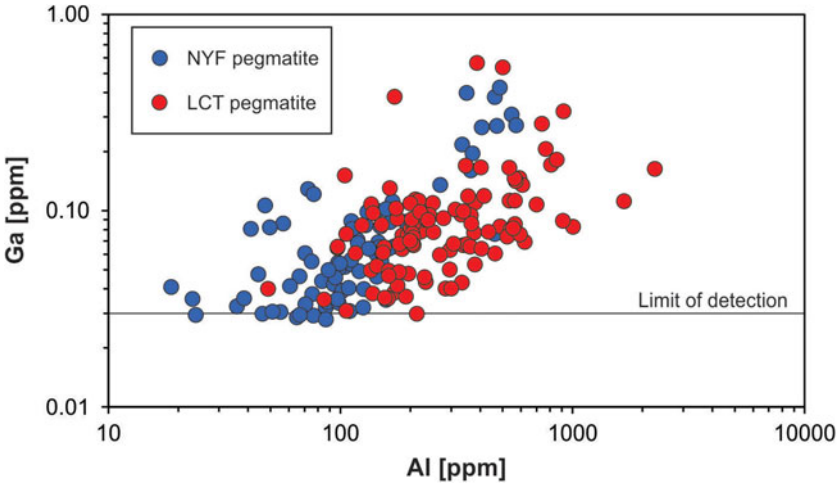

Fig. 13. Aluminium *vs*. Ga in pegmatite quartz of different origin (data from Müller *et al.*, 2021; NYZ = Nb/Y/F-pegmatite, LCT = Li/Cs/Ta-pegmatite according to Černỳ and Ercit, 2005).

epithermal ore deposits. Antimony was measured at concentrations from <5 to ~120 ppm and concentrations fluctuated dramatically among quartz generations and growth zones. Similarly, Monnier *et al.* (2021) found highest Sb contents (up to 200 ppm) in quartz from stibnite-bearing veins, considerably higher than the values measured in quartz unrelated to Sb mineralisation (mainly ≤ 1 ppm). The lack of a consistent relationship between Sb and other trace elements in quartz lead to the conclusion that Sb incorporation in quartz is probably controlled by the content of Sb in the mineralising fluid (Rusk *et al.*, 2011; Pacák *et al.*, 2019; Li *et al.*, 2020; Monnier *et al.*, 2021). Therefore, the Sb content in quartz might be used as a potential indicator for tracing Sb deposits.

Niobium, tantalum, uranium and thorium

For a number of elements the nature of incorporation into quartz is very difficult to determine. In particular these are elements that are present in extremely low concentrations and sometimes below the detection limit of some trace-element analytical methods (e.g. U, Th, Nb and Ta). It can be assumed that the ions are either too large to substitute for the small Si^{4+} ion in the quartz lattice or that they are not soluble in the mineralising fluids that accumulate in fluid inclusions. This can be observed for the immobile elements niobium and tantalum in quartz of Nb–Ta mineralisation, where the extreme low concentrations of these trace elements in associated quartz do not reflect the mineralisation and, therefore, cannot be used as petrogenetic indicators (Götze *et al.*, 2004).

Uranium and thorium are two elements that are typically present in very low concentrations in quartz. Quartz from magmatic, metamorphic rocks and pegmatites has U and Th contents at sub-ppm levels (e.g. Gerler, 1990; Blankenburg *et al.*, 1994; Götze *et al.*, 2004; Götze, 2009). These characteristic low concentrations in quartz can be explained by the fact that the crystal-chemical properties of U and Th (in particular ion sizes) prevent a substitutional incorporation into the quartz structure. The correlation of the U and Th concentrations (Fig. 17a) indicates that traces of both elements are situated on interstitial places in the lattice or bound on submicroscopic mineral inclusions (e.g. on grain boundaries).

Unusually high U concentrations of up to >70 ppm were detected in some microcrystalline quartz and even in macrocrystalline quartz of agates from different worldwide occurrences (Götze *et al.*, 2009, 2015a). Results of CL spectroscopy indicate that U is incorporated into quartz as uranyl ions (UO_2^{2+}), which are bound to the silica surface (Götze *et al.*, 2015a). The presence of uranyl ions can be confirmed easily by its characteristic green luminescence (compare Fig. 10). Recent data confirmed the binding mechanism of uranyl silicate complexes in microcrystalline SiO_2 and suggested a new mechanism of uranium deposition (Fig. 17b; Pan *et al.*, 2021). This model involves uranyl co-precipitation during silicification without the putative reduction process and provided new aspects concerning the formation of uranium deposits.

OH

In addition to water contained in fluid or melt inclusions, quartz may incorporate different amounts of OH point defects in its structure (e.g. Kats, 1962; Bambauer *et al.*, 1962; Chakraborty and Lehmann, 1976; Stalder, 2021). The specific OH defects can be distinguished and quantified by Infrared (IR) spectroscopy based on their characteristic absorption bands. The most common type is the Al–OH defect followed by the Li–OH defect, whereas B–OH and hydrogarnet defects (4H) are less common. Systematic investigations of OH contents in different quartz types revealed that the incorporation of OH defects depends on the specific conditions of formation, but shows no correlation with the amount of molecular water incorporation (Baron *et al.*, 2015; Jaeger *et al.*, 2019; Stalder, 2021).

Quartz from granitic systems may show large variations in OH content with average values of ca. 20 wt. ppm (Stalder, 2021). It has been shown that Variscan samples with 20–35 wt. ppm OH contents have much higher values than Proterozoic samples from Scandinavia with ~3 wt. ppm (Müller and Koch-Müller, 2009; Stalder *et al.*, 2017; Potrafke *et al.*, 2020). Granitic pegmatites contain average OH contents of ca. 20 wt. ppm (Müller and Koch-Müller, 2009). OH contents of up to 13 wt. ppm (average of 6 wt. ppm) were determined for quartz from felsic volcanic rocks. Individual phenocrysts can show strong zoning with a decrease in OH from core to rim (Tollan *et al.*, 2019; Jollands *et al.*, 2020). Hydrothermal quartz crystals are also heterogeneous with respect to the OH content (0–225 wt. ppm) with the highest concentrations in the crystal centre (Kats, 1962; Chakraborty and Lehmann, 1976). The lowest OH contents (mostly <5 wt. ppm) were measured in quartz from metamorphic rocks (Müller and Koch-Müller, 2009; Stalder *et al.*, 2017).

A thorough review about OH defects in quartz has been given recently by Stalder (2021).

https://doi.org/10.1180/mgm.2021.72 Published online by Cambridge University Press

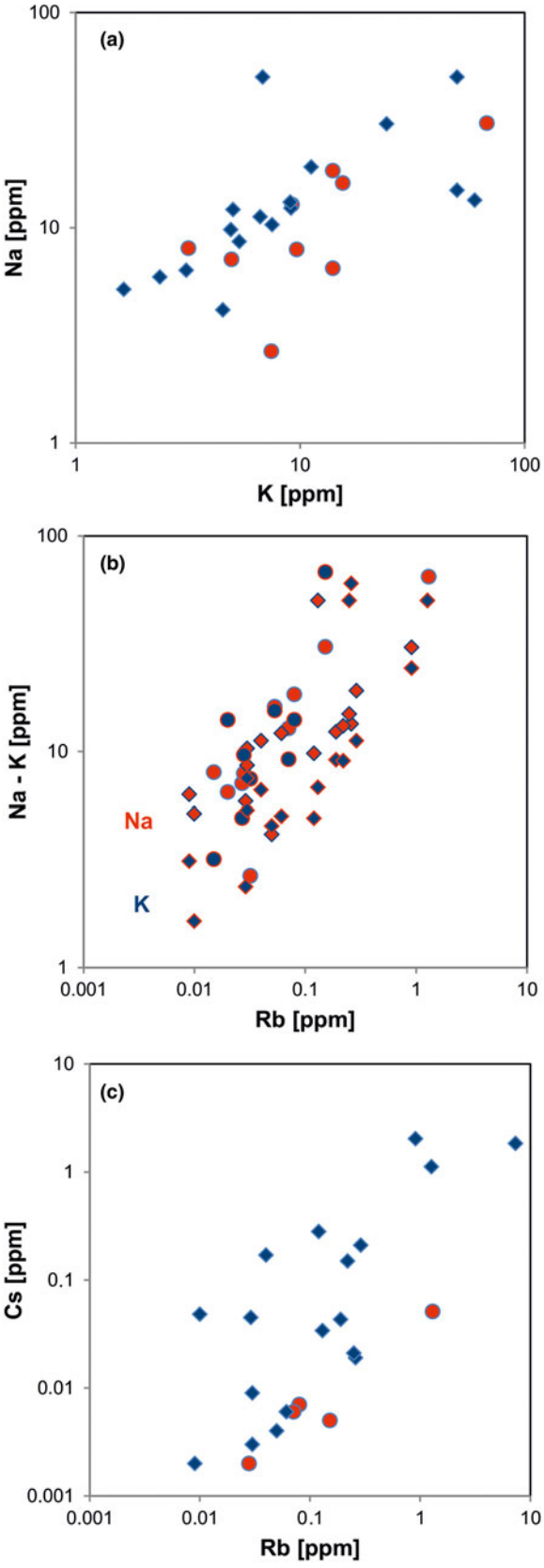

Fig. 14. Contents of alkali elements in quartz: (a) K *vs*. Na; (b) Rb *vs*. Na (red symbols) and Rb *vs*. K (blue symbols); (c) Rb *vs*. Cs. All log plots show positive trends and similar absolute concentrations of K and Na with nearly 1:1 ratio (circles = hydrothermal quartz, rhombs = pegmatite quartz; data from Götze *et al.* 2004, 2017).

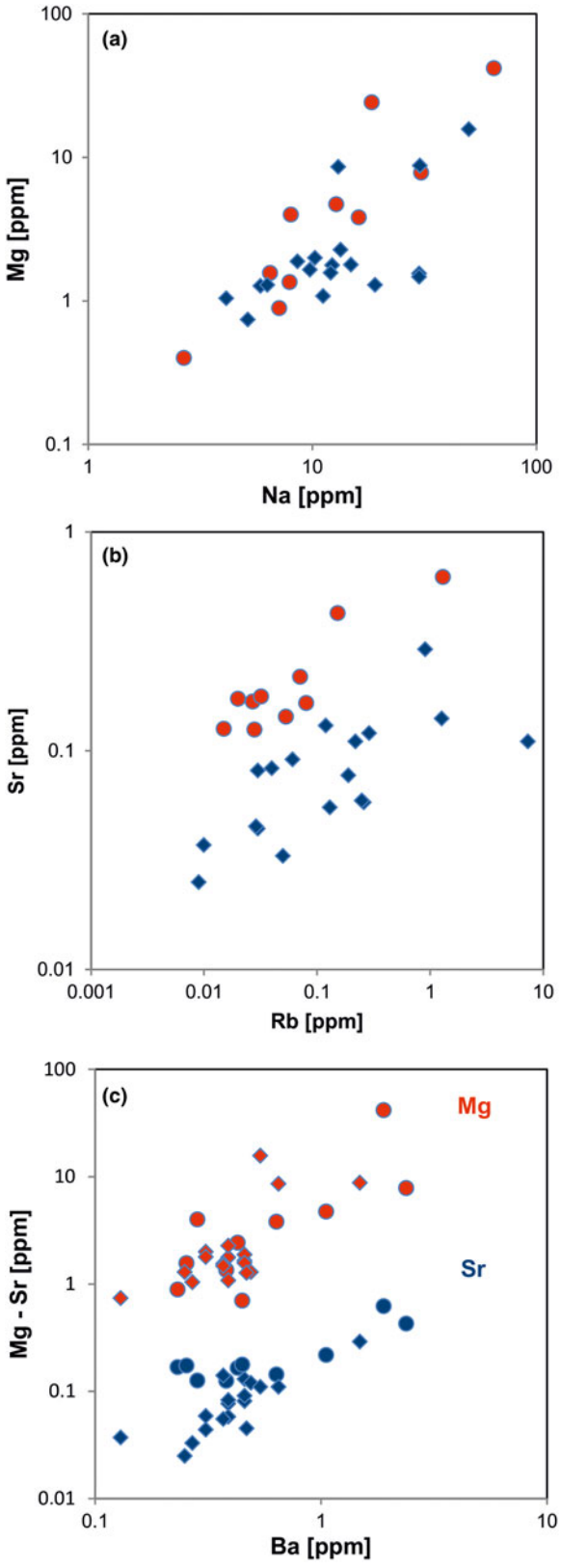

Fig. 15. Contents of alkali and alkali earth elements in quartz: (a) Na *vs*. Mg; (b) Rb *vs*. Sr; (c) Ba *vs*. Mg (red symbols) and Ba *vs*. Sr (blue symbols). All log plots show similar trends with varying absolute concentrations (Mg > Sr); note that pegmatite quartz mostly contains < 0.1 ppm Sr and hydrothermal quartz > 0.1 ppm Sr (circles = hydrothermal quartz, rhombs = pegmatite quartz; data from Götze *et al.* 2004, 2017).

https://doi.org/10.1180/mgm.2021.72 Published online by Cambridge University Press

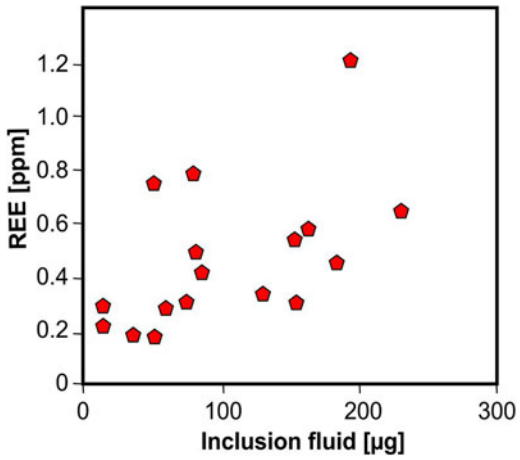

Fig. 16 Bulk REE content in pegmatite quartz plotted *vs*. absolute amount of inclusion fluid in the quartz samples; the correlation trend indicates the preferred accumulation of REE in fluid inclusions; the scatter can be explained by variations of their absolute concentrations in the fluid (data from Götze *et al.*, 2004).

Geological implications of quartz properties

Depending on the specific conditions of formation, quartz can develop characteristic chemical, physical and morphological properties (indicator properties), which range from the atomic scale (point defects) up to macroscopic appearance and crystal morphology. Knowledge about such characteristic features is indispensable for the recognition of any relationships between quartz genesis, its specific properties and possible industrial applications.

Trace elements in quartz as petrogenetic indicators

The trace-element distribution in quartz from different rock types can provide useful information about the formation history of these rocks, as they are highly sensitive to crystallisation and fractionation processes. For instance, trace elements in granites and granitic pegmatites reflect the evolution of the melt and can therefore be used as petrogenetic indicators. Elements such as K, Fe and Ti are geochemically compatible and therefore have the highest concentrations in early formed quartz. In contrast, P, Ge, Rb and Li are relatively incompatible resulting in elevated concentrations in quartz that formed in more evolved granitic melts and/or residual fluids (Schrön *et al.*, 1982, 1988; Larsen *et al.*, 2004; Beurlen *et al.*, 2011; Monnier *et al.*, 2018; Müller *et al.*, 2017; Breiter *et al.*, 2020).

Larsen *et al.* (2004) suggested the Ge/Ti ratio is robust during sub-solidus processes in igneous systems and concluded that it represents a strong index for the evolution of melt differentiation in granitic igneous rocks, and has potential as an igneous geothermometer (Jacomon and Larsen, 2009). The Ge/Ti ratio is a reliable melt fractionation index as Ti in quartz is a function of magma temperature and Ti melt saturation and, thus, decreases with melt differentiation, whereas Ge increases with the melt fractionation degree. A similar behaviour was proposed for the Ge/Fe ratio in quartz (Schrön, 1982, 1988). However, as noted above most of the detected elevated contents of Fe in quartz are related to micro-inclusions of Fe-bearing minerals. Thus, the ratio should not be used for genetic interpretations.

Schrön *et al.* (1988) noticed that elevated Ge concentrations are found in pegmatitic quartz compared to quartz from granites and rhyolites, and established the Ti – Al/10 – 10Ge ternary discrimination diagram, which is still used widely. Most recently Breiter *et al.* (2020) proposed that this diagram does not only enable the discrimination between pegmatitic and granitic quartz, but also permits, to some extent, discrimination between common and rare-metal, and between S- and A-type granites (Fig. 18).

A steady increase in the Ge/Al values in quartz during the transition from magmatic to hydrothermal stages related to rare metal mineralised systems was reported by Müller *et al.* (2018) and Breiter *et al.* (2020). In the case of the Zinnwald/Cinovec Sn–W–Li greisen-type deposit the value of Ge/Al = 0.008 is a discriminator between magmatic and hydrothermal quartz (Müller *et al.*, 2018). In the case of the Panasqueira W deposit, the value of Ge/Al = 0.01 was found to discriminate most of the magmatic quartz from hydrothermal quartz (Breiter *et al.*, 2020).

Breiter and Müller (2009) also detected decreasing Ti content in granitic quartz with increasing fractionation. In contrast, Al contents in quartz increased from the early to the late population independent of the peraluminosity of the melt, resulting in a negative correlation between the Al and Ti contents. Accordingly, the Ti *vs*. Al diagram seems to be the most valuable indicator for the evolution of the melt from which the quartz crystallised (Müller *et al.*, 2002, 2003, 2017; Breiter and Müller, 2009; Jacamon and Larsen, 2009; Breiter *et al.*, 2012; Peterková and Dolejš, 2019). These general trends were also found in quartz from plutons of different geochemical character (Breiter *et al.*, 2013; Hong *et al.*, 2019). The Ge/Ti *vs*. Al/Ti plot shows a positive correlation reflecting the fractionation trend of granitic melts (Breiter *et al.*, 2020).

The trace-element composition of quartz from hydrothermal environments also provides information about primary crystallisation conditions, the mineralisation regime in hydrothermal ore deposits as well as about processes of secondary hydrothermal overprint in different types of host rocks (e.g. Monecke *et al.*, 2002; Rusk *et al.*, 2008, 2012; Jourdan *et al.*, 2009; Luo *et al.*, 2020). For instance, Jourdan *et al.* (2009) reported Al and Li concentrations of more than several hundreds of ppm for distinct growth zones within hydrothermal quartz crystals formed at temperatures of about 300°C or less. These quartz crystals also displayed patterns of cyclic growth under CL. In contrast, quartz crystals formed at temperatures closer to 400°C and without visible cyclic growth have low concentrations of Al, Li and other trace elements.

Such variations were also reported in different quartz generations of ore mineralisation (Rusk *et al.*, 2006, 2008, 2011; Luo *et al.*, 2020). The variations of trace elements such as Ti, Al, Li, K or Na might be related to variations in the pressure and temperature regime, but can also result from fluctuations of the pH and composition of the mineralising solutions or crystallisation rate rather than changes in temperature. Rusk (2012) investigated quartz from almost 30 hydrothermal ore deposits including porphyry-type (Cu–Mo–Au) deposits, orogenic Au deposits, and epithermal deposits and concluded that each of these ore types can be distinguished from one another on the basis of Al and Ti concentrations alone. The temperature dependence of Ti incorporation was used to establish an Al versus Ti discrimination diagram of quartz based on the observation that the Ti content, and to the same extent the Al content, vary systematically among these ore deposit types (Fig. 19).

Most porphyry-type quartz contains 1–200 ppm Ti and 50–500 ppm Al showing a linear correlation with an Al/Ti ratio between 1 and 10. In contrast, quartz from epithermal ore

https://doi.org/10.1180/mgm.2021.72 Published online by Cambridge University Press

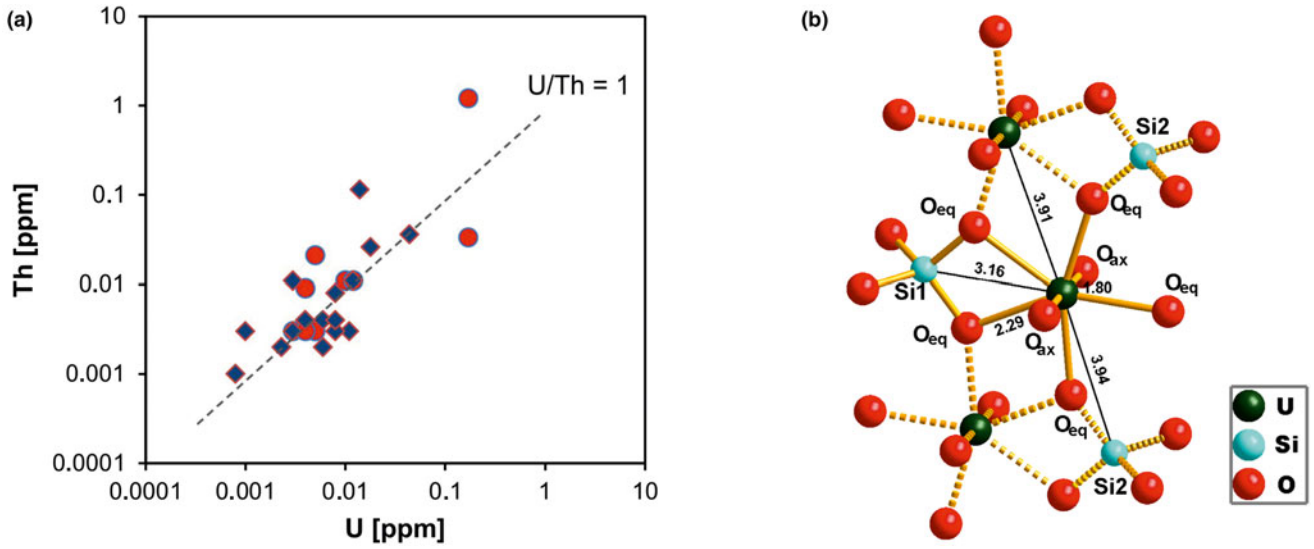

Fig. 17 (a) Th *vs.* U concentrations in quartz samples from different parent rocks and localities (data from Götze *et al.*, 2004, 2017; circles = hydrothermal quartz, rhombs = pegmatite quartz); (b) model of the uranyl–silicate complex in microcrystalline SiO_2 with neighbouring SiO_4 tetrahedra and uranyl polyhedra (modified after Pan *et al.*, 2021).

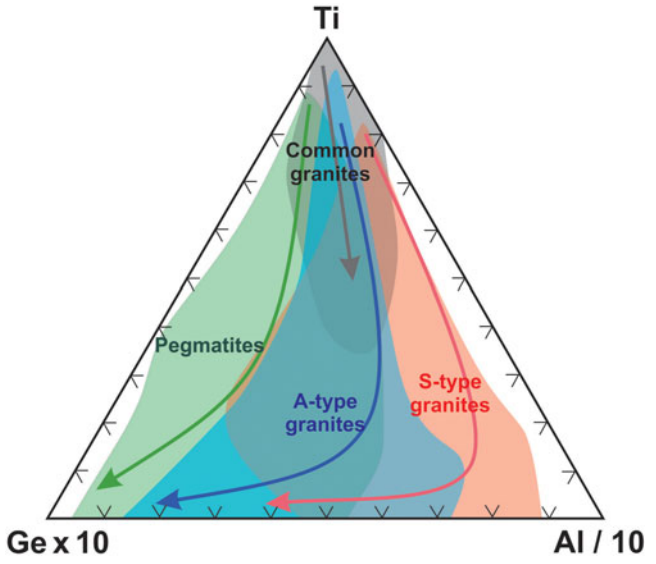

Fig. 18. Triangle for discrimination of S-type granites, A-type granites and pegmatites (modified after Breiter *et al.*, 2020); the arrows indicate evolution trends during magma fractionation.

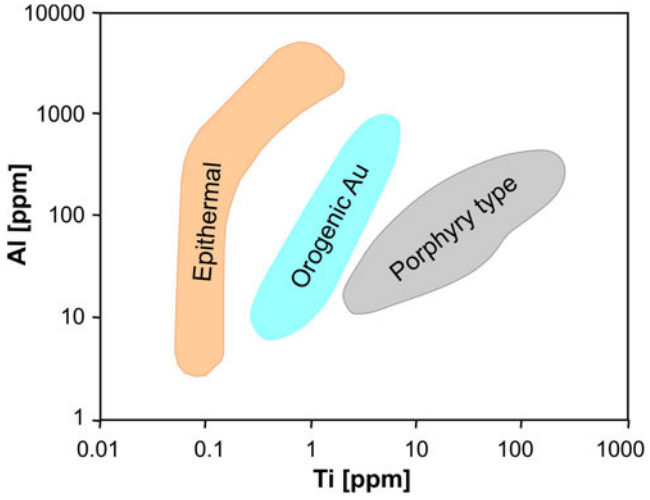

Fig. 19. Log plot of Ti *vs.* Al contents in quartz for the discrimination of hydrothermal quartz originating from epithermal, orogenic Au and porphyry type deposits (modified after Rusk, 2012).

deposits always contains < 3 ppm Ti with a wide scatter of Al between 20 and 4000 ppm (Al/Ti ratios 100–10,000), whereas quartz from orogenic Au deposits mostly has 100–1000 ppm Al and 1–10 ppm Ti (Al/Ti ratio 10–100; Rusk, 2012). These systematic variations in trace-element concentration reflect the different physical and chemical conditions during quartz formation.

Concentrations of REE in quartz can also be used as valuable indicators for geological and/or geochemical processes, as they can reflect the evolution of mineralising fluid and melt compositions. Thus, REE distribution patterns contain important information concerning the primary conditions of quartz formation and also information about secondary effects (Fig. 20). The general shape of the REE distribution and the relationships between light, middle and heavy REE indicate the source of the silica-bearing fluids and the influence of the complexation of the REE during transport (Lipin and McKay, 1986). Moreover, negative and positive anomalies of Ce and Eu can reflect adopted properties from the mineralising fluids and/or variations in redox conditions resulting in a change of the valence state of the ions (Fig. 20).

The hydrothermal quartz samples in Fig. 20a represent different hydrothermal systems and accordingly display characteristic REE distribution patterns. The chondrite-normalised REE distribution pattern of the hydrothermal quartz from the Trans-Atlantic Geotraverse (TAG) mound in the Mid-Atlantic Ridge (Fig. 20a) is bell-shaped with no significant Ce or Eu anomaly. This REE distribution can be related to the origin and evolution of the fluids within the hydrothermal system that is related to

https://doi.org/10.1180/mgm.2021.72 Published online by Cambridge University Press

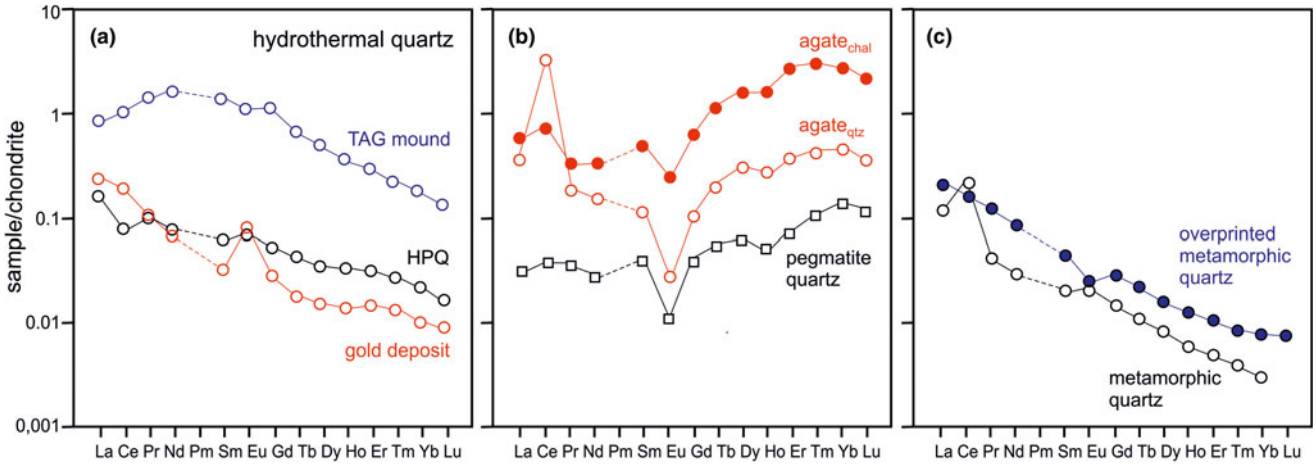

Fig. 20. Chondrite-normalised REE distribution patterns of quartz from different geological environments: (a) hydrothermal quartz from the TAG mound (Mid-Atlantic Ridge), high-purity quartz (HPQ) from Vjazovka (Ural region, Russia) and from the gold deposit Muruntau/Myutenbai (Uzbekistan); (b) pegmatite quartz from Hittero (Norway) and macrocrystalline (agate$_{qtz}$) as well as chalcedony (agate$_{chal}$) of an agate from Hohenstein-Ernstthal (Saxony, Germany) both showing positive Ce-anomalies, negative Eu-anomalies and tetrad effects; (c) metamorphic quartz from the Middle Erzgebirge (Germany) and overprinted counterpart from the area of tin mineralisation; (data from Monecke *et al.*, 2000, 2002; Götze *et al.*, 2004, 2016, 2017).

an actively forming sulfide deposit (Monecke *et al.*, 1999). In contrast, the high-purity quartz from Vjazovka (Ural region, Russia) and the quartz from the hydrothermal gold deposit show typical crustal signatures with a smooth chondrite-normalised REE pattern with decreasing REE concentrations from La to Lu. The negative Ce- and positive Eu-anomalies, result from the evolution of the hydrothermal fluids in the deposits and their interactions with the surrounding wall rocks.

Unusual REE fractionation and the development of tetrad effects (Fig. 20b) can be related to fluid immiscibility and preferential partitioning of the REE between the vapour and coexisting liquid (Monecke *et al.*, 2007). Tetrad effects were observed both in quartz of pegmatites (Götze *et al.*, 2004) and quartz of agates in acidic volcanic rocks (Götze *et al.*, 2016) and probably reflect the participation of volatiles during SiO_2 accumulation and crystallisation. The marked increase of heavy REE indicates the complexation of REE by fluorine or carbonate complexes (Wood, 1990).

The hydrothermal overprint of crystalline host rocks in the vicinity of ore deposits can also result in a change of the REE distribution pattern. An example from quartz in unaltered metamorphic host rocks located distal to the alteration halo within a tin deposit is shown in Fig. 20c. The hydrothermally overprinted quartz shows REE signatures that deviate significantly from the unaltered equivalent. These differences are interpreted to result from the interaction of the pre-existing quartz with the hydrothermal fluids (Monecke *et al.*, 2004).

Several studies have shown that the trace-element composition of quartz can be used to fingerprint the source of detrital quartz grains in clastic sediments (Götze and Zimmerle, 2000). Quartz can retain chemical signatures of the source rocks because of its common occurrence and relative mechanical and chemical stability during sedimentary processes. These geochemical signatures can be used to reveal the origin and provenance of individual quartz grains within sediments. Differences in the distribution of selected trace elements and/or trace-element ratios may be related to inherent characteristics of the source and can be used as discriminating tools (e.g. Dennen, 1967; Hallbauer, 1992; Götze and Lewis, 1994; Müller and Knies, 2013; Ackerson *et al.*, 2015; Stalder *et al.*, 2019).

Another common feature in sedimentary and diagenetic environments is secondary quartz neomorphism as quartz overgrowth cements in sandstones or isolated euhedral quartz crystals in various sedimentary host rock. Authigenic quartz cements play a major role in controlling the hydraulic properties and quality of reservoir sandstones (McBride, 1989). The combination of trace-element studies with other analytical methods (e.g. CL, fluid inclusion and isotope studies) can provide important information about timing of quartz cementation and the burial history of sandstones or concerning temperature and salinity of fluids during precipitation (e.g. Burley *et al.*, 1989; Kelly *et al.*, 2007; Lehmann *et al.*, 2011).

Moreover, some investigations have used complex geochemical and mineralogical studies for the reconstruction of silica sources and diagenetic conditions during the formation of euhedral authigenic quartz crystals in soil, limestones and carbonates, sulfate and salt deposits as well as bituminous coal and lignite (e.g. Füchtbauer, 1961; Grimm, 1962; Fabricius, 1987; Richter, 1971; Friedman and Shukla, 1980; Ruppert *et al.*, 1985; Soong and Blattner, 1986; Götze, 2012b). The resulting mineralogical and geochemical characteristics show that the authigenic quartz from the various sedimentary environments differs clearly from quartz of crystalline rocks and a distinction between quartz from different sedimentary environments is possible.

Interpretation of CL and trace-element data

In general, quartz commonly shows growth zoning in CL, reflecting either variations of the composition of the crystallisation medium (melt or fluid) or changing physicochemical conditions (temperature, Eh, pH). Therefore, combined CL and trace-element studies have significant potential for the reconstruction of crystallisation sequences in magmatic and hydrothermal systems (e.g. Kempe *et al.*, 1999; Landtwing and Pettke, 2005; Müller *et al.*, 2005, 2010; Jourdan *et al.*, 2009; Götte *et al.*, 2011; Audétat, 2013; Mao *et al.*, 2017; Wertich *et al.*, 2018; Wang *et al.*, 2019; Luo *et al.*, 2020; Lan *et al.*, 2021).

Although a correlation of the CL response and the concentration of trace elements has been noted by several authors (e.g. Watt

https://doi.org/10.1180/mgm.2021.72 Published online by Cambridge University Press

et al., 1997; Müller *et al.*, 2003; Rusk *et al.*, 2006, 2008, 2011; Lehmann *et al.*, 2011; Leeman *et al.*, 2012), CL zoning (in particular in panchromatic CL images) in quartz cannot be related solely to variations in the trace-element concentration. For instance, Watt *et al.* (1997) analysed volcanic quartz phenocrysts and xenocrysts by ion microprobe (SIMS) and found higher Al contents in areas of bright CL emission, though they suggested that other factors (e.g. the effect of growth rate on defect density) may also play a major role in controlling CL intensity. Several important aspects limit the possible correlation between the abundance of specific trace elements and visible CL colours or CL zoning.

In summary, it must be emphasised that most of the CL emissions in quartz are related to intrinsic lattice defects and not to trace elements. Therefore, a correlation of CL response to trace elements is often very equivocal. Among the detectable trace elements in quartz only a few of them act as activators for CL emission (compare Table 1). Only Al, Ti and charge compensating alkali ions in hydrothermal and pegmatite quartz sometimes show relations to visible CL behaviour. Most of the inherited trace elements in quartz have no influence on the CL behaviour. To attempt to correlate the concentration of selected trace elements with the visible CL is not reasonable. Spectral CL measurements are necessary and it is only possible to compare trace-element variations with specific individual CL emission bands. In most cases, the bulk CL emission consists of different emission bands and thus, represents a mixture of point defects responsible for the CL signal. Therefore, correlative relations between the CL and single trace elements are very difficult or impossible. In addition, the complexity of the luminescence process and analytical conditions hamper a clear quantitative evaluation of the CL spectra (Habermann, 2002; Götze, 2012a).

The example in Fig. 21 illustrates these complex relationships and demonstrates possible misinterpretations. The hydrothermal quartz crystal exhibits marked zoning in panchromatic CL (Fig. 21a), visible by variations in the intensity of the bulk (cumulative) CL signal (bright and dark zones). Local measurements of the Al content show the dark zones have the highest concentrations (300 ppm) and the bright zones have low (<50 ppm) and not detectable Al concentrations. Attempting to correlate the Al concentration with the panchromatic CL intensity would result in the conclusion that Al correlates negatively with the CL intensity (brightness). However, the corresponding true colour CL image (Fig. 21b) demonstrates that the dark zones exhibit blue CL, whereas bright areas are dominated by yellow CL. Related CL spectra of these zones (Fig. 21c) reveal that the dark areas (transient blue CL) are caused by activation due to Al defects ($[AlO_4/M^+]$ centres), whereas the bright areas (yellow CL) have no relation to trace elements and are exclusively due to structural defects (e.g. STE). In conclusion, the visible zoning in brightness in panchromatic CL (Fig. 21a) is caused mainly by lattice defects and is essentially not related to trace-element variations. This interpretation was only possible by the application of CL spectroscopy.

This example shows the essential problems with CL data, in particular for the interpretation of panchromatic CL images. Even the combination of CL spectroscopy with local trace-element analysis never provides a quantitative relationship between trace elements and the intensity of specific emission bands. For instance, Götte *et al.* (2011) demonstrated the correspondence of Li abundances with $[AlO_4|Li^+]^-$ defects and the transient CL emission at 395 nm in hydrothermal quartz, however they found inconsistencies with a simple causal relationship between Al-Li centres and the 395 nm emission band. They assumed that the conversion of $[AlO_4|Li^+]$ centres to $[AlO_4]^0$ centres by natural irradiation and/or the existence of intrinsic defects such as oxygen deficiency centres can affect the luminescence properties. Similar results were reported by Sittner (2019) for the CL of pegmatite quartz. The 500 nm emission band could clearly be ascribed to structurally incorporated Li, but a clear quantitative correlation between Li concentration and intensity of the 500 nm emission band was missing. The incorporation of other monovalent cations and the charge-compensation of Al^{3+} by electron defects were discussed as possible explanations.

Another problem is the ongoing discussion about the role of Ti as an activator of CL in quartz. Observations about correlations between the Ti content in quartz and the CL intensity resulted in the conclusion that the blue CL emission band at 450 nm might be activated by Ti (e.g. Müller *et al.*, 2002, 2003; Van den Kerkhof *et al.* 2004; Rusk *et al.*, 2008; Drivenes *et al.*, 2016). First attempts have been made to quantify the Ti concentration in quartz by using the intensity of the 450 nm emission band (Leeman *et al.*, 2012). These assumptions are in sharp contrast to previous investigations, which have provided evidence by spectroscopic methods that the blue 450 nm emission can be related to oxygen deficiency centres (ODC) (e.g. Stevens-Kalceff and Phillips, 1995; Skuja, 1998; Stevens-Kalceff, 2009).

Recent studies on quartz of different origin and containing different concentrations of Ti revealed that structural defects not related to trace elements (self-trapped exciton – STE) and also incorporation of Ti into the quartz structure can both activate a blue CL emission at the same position (450 nm, 2.75 eV; unpublished data). The STE-activated CL emission is unstable under the electron beam and in particular detectable in quartz with low Ti contents (e.g. high-purity hydrothermal quartz), whereas high Ti concentrations (e.g. in quartz phenocrysts of rhyolites) result in a stable CL emission (Fig. 22). In conclusion, even in the case of Ti activation of the 450 nm luminescence emission in quartz, the superposition with the STE emission at the same position would prevent any serious quantitative evaluation of the CL signal. A reliable distinction of the two different CL emissions at 450 nm is only possible by time-resolved CL spectroscopy combined with EPR spectroscopy and trace-element analysis of the Ti concentration. This example emphasises that the correlation of CL and trace-element data has to be done with caution.

Conclusions

Quartz is one of the most common minerals in the Earth crust and occurs ubiquitously in magmatic, metamorphic and sedimentary rocks. This common occurrence makes it an important pathfinder mineral for the reconstruction of geological processes and palaeoclimatic conditions as well as the exploration of mineral deposits and other natural resources.

Although quartz has a simple composition and represents a very pure mineral with low abundances of defects and impurities, it develops significant indicator properties depending on its formation history and the influence of secondary processes. Analytical techniques with low detection limits and/or high spatial resolution can provide a wealth of data concerning the real structure and chemistry of natural and synthetic quartz. The analytical combination of CL microscopy and spectroscopy, EPR spectroscopy, as well as spatially resolved trace-element analysis has been demonstrated to characterise the type and abundance of structural defects and trace elements in quartz, and permit

https://doi.org/10.1180/mgm.2021.72 Published online by Cambridge University Press

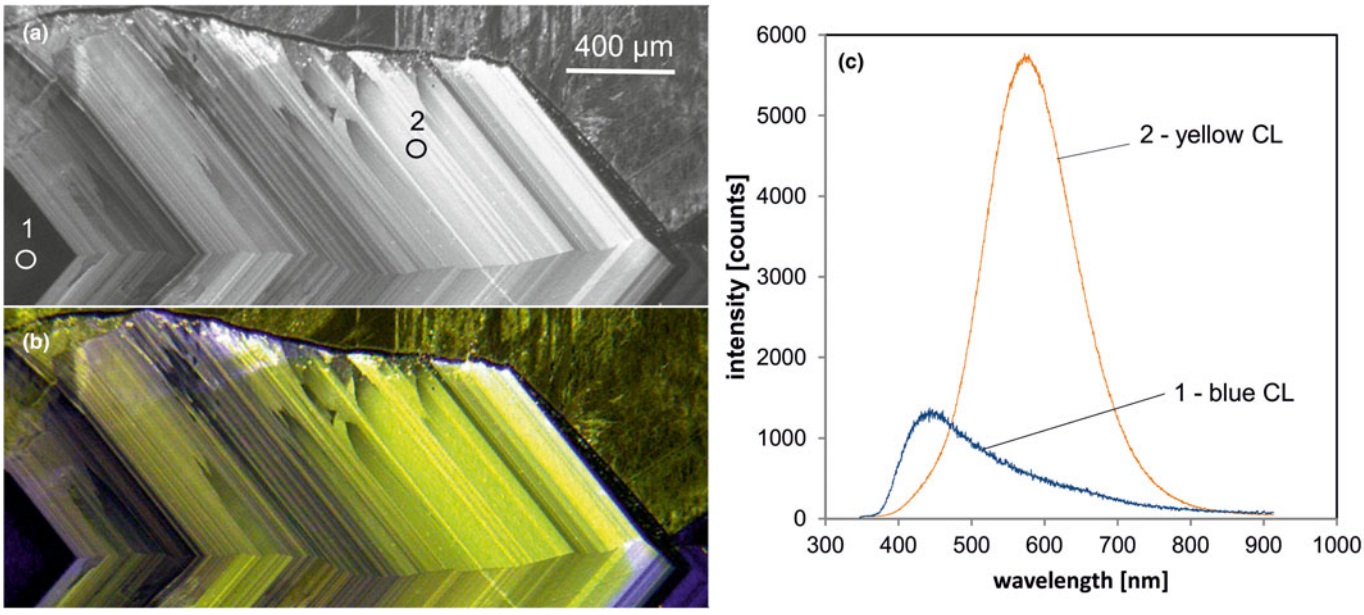

Fig. 21 Photomicrographs of intensely zoned hydrothermal quartz from Chemnitz (Saxony, Germany) in panchromatic CL (a) and true colour optical microscopy–cathodluminescence image (b); the dark luminescent zones in panchromatic CL (blue CL zones in b) have elevated Al concentrations up to 300 ppm, whereas the bright zones in panchromatic CL (yellow in b) have mostly low (< 50 ppm) or no detectable Al contents; Ti concentrations are generally < 10 ppm. (c) The spectra reveal that the blue CL (1) is caused by the incorporation of structural Al ($[AlO_4/M^+]$ centre), the yellow CL (2) is related mainly to structural defects (e.g. STE) and not to trace elements; the circles in (a) mark the positions of spectral CL analyses.

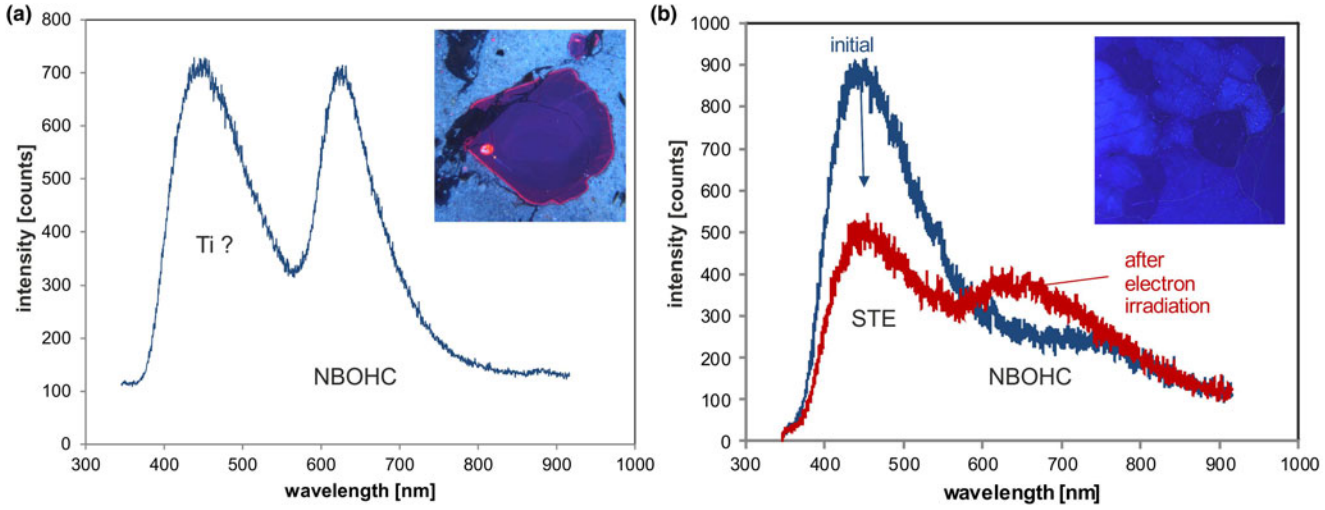

Fig. 22. CL emission spectra of (a) a quartz phenocryst in the Leisnig porphyry (Saxony, Germany) and (b) high-purity quartz from Kuznechikhinsk (Ural, Russia). Both quartz samples exhibit a blue CL (see insets) with a dominant emission band at 450 nm. The blue CL emission band of the Ti-rich quartz phenocryst (up to 80 ppm Ti and paramagnetic $[TiO_4/M^+]^-$ centres) is stable during electron irradiation and can probably be related to the activation by substitutional Ti. In contrast, the intensity of the STE-activated 450 nm emission band of the HPQ quartz (4.52 ppm Ti, no detectable Ti-centres) shows a strong decrease due to electron bombardment.

reconstruction of processes responsible for their formation and secondary effects. Each of these analytical techniques can provide specific information about the point defects and trace-element uptake in quartz.

It has been shown that quartz from different geological settings might have different trace-element composition related to the different supply and mechanisms of incorporation of certain elements. Therefore, trace elements in quartz are important petrogenetic indicators in geosciences. In addition, intrinsic types of point defects detected by EPR can provide valuable genetic information. Cathodoluminescence can help to visualise the real structure of quartz and to relate internal textures to possible formation processes.

However, interpretation of analytical data might be limited by the ability of quartz to regenerate during secondary alteration processes occurring under metamorphic or hydrothermal conditions. Therefore, primary genetic information concerning the real structure or trace-element composition might be obliterated during quartz alteration or regeneration (Kempe *et al.*, 2012). In these cases care has to be taken when interpreting the genetic

https://doi.org/10.1180/mgm.2021.72 Published online by Cambridge University Press

information encoded. Distinction of features related to primary growth or secondary alteration of quartz is not simple and requires application of complementary analytical techniques.

Acknowledgements. We are grateful for analytical help and productive discussions from Jonathan Sittner, Axel Renno and Ulf Kempe (Freiberg, Germany), Rudolf Mashkovtsev (Novosibirsk, Russia) as well as Marion Stevens-Kalceff (Sidney, Australia). We acknowledge comprehensive reviews by Rune B. Larsen, K. Breiter and an anonymous reviewer, which improved the quality of the manuscript significantly.

Supplementary material. To view supplementary material for this article, please visit https://doi.org/10.1180/mgm.2021.72

References

Ackerson M.R., Tailby N.D. and Watson E.B. (2015) Trace elements in quartz shed light on sediment provenance. *Geochemistry, Geophysics, Geosystems*, **16**, 1894–1904.

Alessi A., Agnello S., Buscarino G., Pan Y. and Mashkovtsev R.I. (2014) EPR on radiation-induced defects in SiO_2. Pp. 255–298 in: *Applications of EPR in Radiation Research* (A. Lund and M. Shiotani, editors). Springer, Berlin.

Alonso P.J., Halliburton L.E., Kohnke E.E. and Bossoli R.B. (1983) X-ray induced luminescence in crystalline SiO_2. *Journal of Applied Physics*, **54**, 5369–5375.

Audétat A. (2013) Origin of Ti-rich rims in quartz phenocrysts from the Upper Bandelier Tuff and the Tunnel Spring Tuff, southwestern USA. *Chemical Geology*, **360–361**, 99–104.

Bailey P. and Weil J.A. (1991) EPR study of the $[SiO_4/Li]^0$ center in alpha-quartz. *Journal of the Chemical Society-Faraday Transactions*, **87**, 3143–3146.

Bailey P. and Weil J.A. (1992a) EPR of $[TiO_4/Li]B^0$ and related centers in X-irradiated alpha-quartz. *Journal of Physics and Chemistry of Solids*, **53**, 601–610.

Bailey P. and Weil J.A. (1992b) The EPR spectral parameters and dynamic properties of the center $[TiO_4/Na]^0_A$ in X-irradiated alpha-quartz. *Journal of Physics and Chemistry of Solids*, **53**, 309–318.

Bailey P., Pawlik T., Sothe H., Spaeth J.-M. and Weil J.A. (1992) $[TiO_4]^-$ in α-quartz studied by low-temperature electron paramagnetic resonance. *Journal of Physics Condensed Matters*, **4**, 4063–4073.

Bambauer H.U. (1961) Spurenelemente und γ-Farbzentren in Quarzen aus Zerrklüften der Schweizer Alpen. *Schweizerische Mineralogische Petrographische Mitteilungen*, **41**, 335–367.

Bambauer H.U., Brunner G.O. and Laves F. (1962) Wasserstoff-Gehalte in Quarzen aus Zerrklüften der Schweizer Alpen. *Schweizerische Mineralogische Petrographische Mitteilungen*, **42**, 221–236.

Baron M.A., Stalder R., Konzett J. and Hauzenberger C.A. (2015) Formation conditions of quartz recorded by OH-point defects – experimental and analytical approach. *Physics and Chemistry of Minerals*, **42**, 53–62.

Baur W.H. (2009) In search of the crystal structure of low quartz. *Zeitschrift für Kristallographie*, **224**, 580–592.

Bershov L.V. (1970) Isomorphism of titanium in natural minerals. *Izvestya Akademii Nauk SSSR, Seria Geologizna*, **12**, 47–54 [in Russian].

Beurlen H., Müller A., Silva D. and Da Silva M.R.R. (2011) Petrogenetic significance of LA–ICP–MS trace-element data on quartz from the Borborema pegmatite province, Northeast Brazil. *Mineralogical Magazine*, **75**, 2703–2719.

Blankenburg H.-J., Götze J. and Schulz H. (1994) *Quarzrohstoffe*. Deutscher Verlag für Grundstoffindustrie, Leipzig-Stuttgart, Germany, 296 pp.

Botis S.M. and Pan Y. (2009) First-principles calculations on the $[AlO_4/M^+]^0$ (M = H,Li,Na,K) defects in quartz and crystal-chemical controls on the uptake of Al. *Mineralogical Magazine*, **73**, 537–550.

Botis S.M. and Pan Y. (2011) Modeling of $[AlO_4/Li^+]^+$ paramagnetic defects in α-quartz. *Canadian Journal of Physics*, **89**, 809–816.

Botis S.M., Nokhrin S.M., Pan Y., Xu Y. and Bonli T. (2005) Natural radiation-induced damage in quartz. I. Correlations between cathodoluminescence colors and paramagnetic defects. *The Canadian Mineralogist*, **43**, 1565–1580.

Botis S.M., Pan Y., Bonli T., Xu Y., Zhang A., Nokhrin S. and Sopuck V. (2006) Natural radiation-induced damage in quartz. II. Distribution and implications for uranium mineralization in the Athabasca Basin, Saskatchewan, Canada. *The Canadian Mineralogist*, **44**, 1387–1402.

Botis S.M., Pan Y., Nokhrin S. and Nilges M.J. (2008) Natural radiation induced damage in quartz. III. A new ozonide radical in drusy quartz from the Athabasca basin, Saskatchewan. *The Canadian Mineralogist*, **46**, 125–138.

Bottrell S.H., Yardley B. and Buckley F. (1988) A modified crush-leach method for the analysis of fluid inclusion electrolytes. *Bulletin de Minéralogy*, **111**, 279–290.

Breiter K. and Müller A. (2009) Evolution of rare-metal granitic magmas documented by quartz chemistry. *European Journal of Mineralogy*, **21**, 335–346.

Breiter K., Svojtka M., Ackerman L. and Švecová K. (2012) Trace element composition of quartz from the Variscan Teplice caldera (Krušné Hory/Erzgebirge Mts., Czech Republic/Germany): insights into the volcano-plutonic complex evolution. *Chemical Geology*, 326–327, 36–50.

Breiter K., Ackerman L., Svojtka M. and Müller A. (2013) Behavior of trace elements in quartz from plutons of different geochemical signature: A case study from the Bohemian Massif, Czech Republic. *Lithos*, 175–176, 54–67.

Breiter K., Ackerman L., Ďurišová J., Svojtka M. and Novák M. (2014) Trace element composition of quartz from different types of pegmatites: a case study from the Moldanubian Zone of the Bohemian Massif (Czech Republic). *Mineralogical Magazine*, **78**, 703–722.

Breiter K., Ďurišová J. and Dosbaba M. (2020) Chemical signature of quartz from S- and A-type rare-metal granites – A summary. *Ore Geology Reviews*, **125**, 103674.

Burley S.D., Mullis J. and Matter A. (1989) Timing diagenesis in the Tartan Reservoir (UK North Sea): constraints from combined cathodoluminescence microscopy and fluid inclusion studies. *Marine Petrology and Geology*, **6**, 98–120.

Cerin D., Götze J. and Pan Y. (2017) Radiation induced damage in quartz at the Arrow uranium deposit, southwestern Athabasca Basin, Saskatchewan. *The Canadian Mineralogist*, **55**, 457–472.

Černỳ P. and Ercit T.S. (2005) The classification of granitic pegmatites revisited. *The Canadian Mineralogist*, **43**, 2005–2006.

Chakraborty D. and Lehmann G. (1976) Distribution of OH in synthetic and natural quartz crystals, *Journal of Solid State Chemistry*, **17**, 305–31.

Claridge R.F., Kryliouk O.M., Weil J.A. and Williams J.A. (2008) Paramagnetic Ge-Li centres in alpha quartz revisited: The $D_{Li}([GeO_4/Li\ ]^0_D$ centre. *Canadian Journal of Physics*, **86**, 1303–1311.

Cohen A.J. (1956) Color centers in alpha-quartz. Part I. Smoky quartz. *Journal of Chemistry and Physics*, **25**, 908–914.

Cohen A.J. (1985) Amethyst color in quartz, the result of radiation protection involving iron. *American Mineralogist*, **70**, 1180–1185.

Cohen A.J. and Makar L.N. (1985) Dynamic biaxial absorption spectra of Ti^{3+} and Fe^{2+} in a natural rose quartz crystal. *Mineralogical Magazine*, **49**, 709–715.

Cox R.T. (1976) ESR of an S = 2 centre in amethyst quartz and its possible identification as the d^4 ion Fe^{4+}. *Journal of Physics C, Solid State Physics*, **9**, 3355–3361.

Cox R.T. (1977) Optical absorption of the d^4 ion Fe^{4+} in pleochroic amethyst quartz. *Journal of Physics C, Solid State Physics*, **10**, 4631–4643.

Cressey G., Henderson C.M.B. and Van der Laan G. (1993) Use of L-edge X-ray absorption spectroscopy to characterize multiple valence states of 3d transition metals; a new probe for mineralogical and geochemical research. *Physics and Chemistry of Minerals*, **20**, 111–119.

Daniels M.E. and Morton I.P. (1981) The thermal conductivity and magnetization of iron-doped quartz crystals. *Physica*, **108B**, 867–868.

Davis P.H. and Weil J.A. (1978) Silver atom center in alpha-quartz. *Journal of the Physics and Chemistry of Solids*, **39**, 775–80.

Dedushenko S.K., Makhina I.B., Marin A.A., Mukhanov V.A. and Perfiliev Y.D. (2004) What oxidation state of iron determines the amethyst colour? *Hyperfine Interaction*, **156**(157), 417–422.

Demars C., Pagel M., Deloule E. and Blanc P. (1996) Cathodoluminescence of quartz from sandstones: Interpretation of the UV range by determination of trace element distributions and fluid-inclusion P-T-X properties in authigenic quartz. *American Mineralogist,* **81**, 891–901.

Dennen W.H. (1967) Trace elements in quartz as indicators of provenance. *Geological Society of America Bulletin*, **78**, 125–130.

Di Benedetto F., D'Acapito F., Fornaciai G., Montegrossi G., Pardi L., Tesi S. and Romanelli M. (2009) Fe K-edge XAS study of amethyst. *Physics and Chemistry of Minerals*, **37**, 283–289.

Di Benedetto F., Giaccherini A., Montegrossi G., Pardi L.A., Zoleo A., Capolupo F., Innocenti M., Lepore G.O., d'Acapito F., Capacci F., Poli C., Iaia T.E., Buccianti A. and Romanelli M. (2019) Chemical variability of artificial stone powders in relation to their health effects. *Scientific Reports*, **9**, 6531.

Di Benedetto F., Giaccherini A., Romanelli M. *et al.* (2021) A study of radicals in industrial raw cristobalite powders. *Physics and Chemistry of Minerals*, **48**, 9.

Dickson R.S. and Weil J.A. (1990) The magnetic properties of the oxygen-hole aluminum centres in crystalline SiO_2. IV. $[AlO_4/Na^+]^+$. *Canadian Journal of Physics*, **68**, 630–642.

Dickson R.S., Weil J.A. and Davis P.H. (1991) The paramagnetic germanium sodium impurity centers $[GeO_4/Na]^0_A$ and $[GeO_4/Na]^0_C$ in alpha-quartz. *Canadian Journal of Physics*, **69**, 761–779.

Dong G., Morrison G. and Jaireth S. (1995) Quartz textures in epithermal veins, Queensland – Classification, origin, and implication. *Economic Geology*, **90**, 1841–1856.

Donnay J.D.H. and Le Page Y. (1978) The vicissitudes of the low-quartz crystal setting or the pitfalls of enantiomorphism. *Acta Crystallographica,* **A34**, 584–594.

Drivenes K., Larsen R.B., Müller A. and Sørensen B.E. (2016) Crystallization and uplift path of late Variscan granites evidenced by quartz chemistry and fluid inclusions: Example from the Land's End granite, SW England. *Lithos*, **252–253**, 57–75.

Entzian W. and Ahlgrimm C. (1983) Comparative studies about the cathodoluminescence of SiO_2. *Wissenschaftliche Zeitschrift Universität Rostock, Naturwissenschaftliche Reihe* **32**, 27–29 [in German].

Fabricius J. (1987) Natural Na-K-Mg-Cl solutions and solid derivatives trapped in euhedral quartz from Danish Zechstein salt. *Chemical Geology*, **61**, 95–112.

Feigl F.J. and Anderson J.H. (1970) Defects in crystalline quartz: electron paramagnetic resonance of E' vacancy centers associated with germanium impurities. *Journal of Physics and Chemistry of Solids*, **31**, 575–596.

Friebele E.J., Griscom D.L., Stapelbroek M. and Weeks R.A. (1979) Fundamental defect centers in glass: the peroxy radical in irradiated, high-purity, fused silica. *Physical Review Letters*, **42**, 1346–1348.

Friedman G.M. and Shukla V. (1980) Significance of authigenic quartz euhedra after sulphates; example from the Lockport formation (Middle Silurian) from New York. *Journal of Sedimentary Research*, **50**, 1299–1304.

Fubini B., Giamello E., Volante M. and Bolis V. (1990) Chemical functionalities at the silica surface determining its reactivity when inhaled. Formation and reactivity of surface radicals. *Toxicology and Health*, **6**, 571–598.

Füchtbauer H. (1961) Zur Quarzneubildung in Erdöllagerstätten. *Erdöl und Kohle*, **14**, 169–173.

Gaillou E., Delaunay A., Rondeau B., Bouhnik-le-Coz M., Fritsch E., Cornen G. and Monnier C. (2008) The geochemistry of gem opals as evidence of their origin. *Ore Geology Reviews*, **34**, 113–126.

Gerler J. (1990) *Geochemische Untersuchungen an hydrothermalen, metamorphen, granitischen und pegmatitischen Quarzen und deren Flüssigkeitseinschlüssen*. PhD thesis, University Göttingen, Germany.

Gerler J. and Schnier C. (1989) Neutron activation analysis of liquid inclusions exemplified by a quartz sample from the Ramsbeck Mine, F.R.G. *Nuclear Geophysics*, **3**, 41–48.

Ghazi A.M., Vanko D.A., Roedder E. and Seeley R.C. (1993) Determination of rare earth elements in fluid inclusions by inductively coupled plasma-mass spectrometry (ICP-MS). *Geochimica et Cosmochimica Acta*, **57**, 4513–4516.

Giordano L., Sushko P.V., Pacchioni G. and Shluger A.L. (2007) Optical and EPR properties of point defects at a crystalline silica surface: ab initio embedded-cluster calculations. *Physical Reviews B*, **75**, 24109–24119.

Glazer A.M. (2018) Confusion in the description of the quartz structure yet again. *Journal of Applied Crystallography*, **51**, 915–918.

Goldsmith D.F. (1994) Health effects of silica dust exposure. Pp. 545–595 in: *Silica: Physical Behavior, Geochemistry, and Materials Applications* (P.J. Heaney, C.T. Prewitt, and G.V. Gibbs, editors). Reviews in Mineralogy, **Vol. 29**. Mineralogical Society of America, Washington DC.

Goreva J.S., Ma C. and Rossman G.R. (2001) Fibrous nanoinclusions in massive rose quartz: The origin of rose coloration. *American Mineralogist*, **86**, 466–472.

Gorobets B.S. and Rogozine A.A. (2002) *Luminescent Spectra of Minerals*. RPC VIMS, Moscow, Russia.

Gorton N.T., Walker G. and Burley S.D. (1996) Experimental analysis of the composite blue CL emission in quartz. *Journal of Luminescence*, 72–74, 669–671.

Götte T. (2016) Trace element composition of authigenic quartz in sandstones and its correlation with fluid–rock interaction during diagenesis. Pp. 435 in: *Reservoir Quality of Clastic and Carbonate Rocks: Analysis, Modelling and Prediction*. (P.J. Armitage, A.R. Butcher, J.M. Churchill, A.E. Csoma, C. Hollis, R.H. Lander, J.E. Omma, and R.H. Worden, editors.) Geological Society Special Publications, London, Great Britain.

Götte T., Pettke T., Ramseyer K., Koch-Müller M. and Mullis J. (2011) Cathodoluminescence properties and trace element signature of hydrothermal quartz: A fingerprint of growth dynamics. *American Mineralogist*, **96**, 802–813.

Götze J. (2009) Chemistry, textures and physical properties of quartz – geological interpretation and technical application. *Mineralogical Magazine*, **73**, 645–671.

Götze J. (2012a) Application of cathodoluminescence (CL) microscopy and spectroscopy in geosciences. *Microscopy and Microanalysis*, **18**, 1270–1284.

Götze J. (2012b) Mineralogy, Geochemistry and cathodoluminescence of authigenic quartz from different sedimentary rocks. Pp. 287–306 in: *Quartz: Deposits, Mineralogy and Analytics*. (J. Götze and R. Möckel, editors). Springer Geology, Heidelberg-New York-Dordrecht-London.

Götze J. and Hanchar J. (2018) *Atlas of Cathodoluminescence (CL) Microtextures*. GAC Miscellaneous Publication No. 10. Geological Association of Canada, St. John's, Newfoundland and Labrador, Canada.

Götze J. and Lewis R. (1994) Distribution of REE and trace elements in size and mineral fractions of high purity quartz sands. *Chemical Geology*, **114**, 43–57.

Götze J. and Möckel R. (editors) (2012) *Quartz: Deposits, Mineralogy and Analytics*. Springer Geology, Heidelberg-New York-Dordrecht-London.

Götze J. and Plötze M. (1997) Investigation of trace-element distribution in detrital quartz by Electron Paramagnetic Resonance (EPR). *European Journal of Mineralogy*, **9**, 529–537.

Götze J. and Zimmerle W. (2000) Quartz and silica as guide to provenance in sediments and sedimentary rocks. *Contributions to Sedimentary Petrology*, **21**, 91 p.

Götze J., Plötze M., Fuchs H. and Habermann D. (1999) Defect structure and luminescence behaviour of agate – results of electron paramagnetic resonance (EPR) and cathodoluminescence (CL) studies. *Mineralogical Magazine*, **63**, 149–163.

Götze J., Plötze M. and Habermann D. (2001a) Cathodoluminescence (CL) of quartz: origin, spectral characteristics and practical applications. *Mineralogy and Petrology*, **71**, 225–250.

Götze J., Plötze M., Tichomirowa M., Fuchs H. and Pilot J. (2001b) Aluminium in quartz as indicator for the temperature of formation of agate. *Mineralogical Magazine*, **65**, 400–406.

Götze J., Plötze M., Graupner T., Hallbauer D.K. and Bray C. (2004) Trace element incorporation into quartz: a combined study by ICP-MS, electron spin resonance, cathodoluminescence, capillary ion analysis and gas chromatography. *Geochimica et Cosmochimica Acta*, **68**, 3741–3759.

Götze J., Plötze M. and Trautmann T. (2005) Structure and luminescence characteristics of quartz from pegmatites. *American Mineralogist*, **90**, 13–21.

Götze J., Möckel R., Kempe U., Kapitonov I. and Vennemann T. (2009) Origin and characteristics of agates in sedimentary rocks from the Dryhead area, Montana/USA. *Mineralogical Magazine*, **73**, 673–690.

Götze J., Schrön W., Möckel R. and Heide K. (2012) The role of fluids in the formation of agate. *Geochemistry*, **72**, 283–286.

Götze J., Hanchar J., Schertl. H.-P., Neuser D.K. and Kempe U. (2013) Optical microscope-cathodoluminescence (OM–CL) imaging as a powerful tool to reveal internal textures of minerals. *Mineralogy and Petrology*, **107**, 373–392.

https://doi.org/10.1180/mgm.2021.72 Published online by Cambridge University Press

Götze J., Gaft M. and Möckel R. (2015a) Uranium and uranyl luminescence in agate/chalcedony. *Mineralogical Magazine*, **79**, 983–993.

Götze J., Pan Y., Stevens-Kalceff M., Kempe U. and Müller A. (2015b) Origin and significance of the yellow cathodoluminescence (CL) of quartz. *American Mineralogist*, **100**, 1469–1482.

Götze J., Möckel R., Vennemann T. and Müller A. (2016) Origin and geochemistry of agates from Permian volcanic rocks of the Sub-Erzgebirge basin (Saxony, Germany). *Chemical Geology*, **428**, 77–91.

Götze J., Pan Y., Müller A., Kotova E.L. and Cerin D. (2017) Trace element compositions and defect structures of high-purity quartz from the Southern Ural region, Russia. *Minerals*, **7**, 189.

Götze J., Möckel R. and Pan Y. (2020) Mineralogy, geochemistry and genesis of agates – a review. *Minerals*, **10**, 1037.

Grew E.S. and Hinthorne J.R. (1983) Boron in sillimanite. *Science*, **221**, 547–549.

Griffiths J.H.E., Owen J. and Ward I.M. (1954) Paramagnetic resonance in neutron-irradiated diamond and smoky quartz. *Nature*, **173**, 439–442.

Grimm W.-D. (1962) Idiomorphe Quarze als Leitmineralien für salinare Fazies. *Erdöl und Kohle*, **15**, 880–887.

Griscom D.L. (1985) Defect structure of glasses. *Journal of Non-Crystalline Solids*, **73**, 51–77.

Günther D., Audétat A., Frischknecht R. and Heinrich C.A. (1998) Quantitative analysis of major, minor and trace elements in fluid inclusions using laser ablation–inductively coupled plasma mass spectrometry. *Journal of Analytical Atomic Spectrometry*, **13**, 263–270.

Habermann D. (2002) Quantitative cathodoluminescence (CL) spectroscopy of minerals: possibilities and limitations. *Mineralogy and Petrology*, **76**, 247–259.

Hallbauer D.K. (1992) The use of selected trace elements in vein quartz and quartz pebbles in identifying processes of formation and source rocks. *Proceedings Geological Society South Africa, Bloemfontein*, 157–159.

Halliburton L.E., Hantehzadeh M.R., Minge J., Mombourquette M.J. and Weil J.A. (1989) EPR study of Fe^{3+} in alpha quartz: a reexamination of the lithium-compensated center. *Physical Reviews B*, **40**, 2076–2081.

Han C.S. and Choh S.H. (1989) EPR study of iron centers in natural amethyst. *Journal of the Korean Physical Society*, **22**, 241–252.

Harben P.W. (2002) *The Industrial Mineral Handbook – A Guide to Markets, Specifications and Prices*, 4th Edition. Industrial Mineral Information. Worcester Park, Surrey, UK 412 p.

Heaney P.J. and Davis A.M. (1995) Observation and origin of self-organized textures in agates. *Science*, **269**, 1562–1565.

Hong W., Cooke D.R., Zhang L., Fox N. and Thompson J. (2019) Cathodoluminescence features, trace elements, and oxygen isotopes of quartz in unidirectional solidification textures from the Sn-mineralized Heemskirk granite, western Tasmania. *American Mineralogist*, **104**, 100–117.

Hu B., Pan Y., Botis S., Rogers B., Kotzer T. and Yeo G. (2008) Radiation-induced defects in drusy quartz, Athabasca Basin, Canada: A new aid to exploration of uranium deposits. *Economic Geology*, **103**, 1571–1580.

Huang R. and Audétat A. (2012) The titanium-in-quartz (TitaniQ) thermobarometer: A critical examination and re-calibration. *Geochimica et Cosmochimica Acta*, **84**, 75–89.

Hutton D.R. and Troup G.J. (1966) Paramagnetic resonance centres in amethyst and citrine quartz. *Nature*, **211**, 621.

Isoya J. and Weil J.A. (1979) Uncompensated titanium(3+) center in alpha-quartz. *Physica status solidi a,* **52**, K193–K196.

Isoya J., Weil J.A. and Claridge R.F.C. (1978) The dynamic interchange and relation between germanium centers in alpha-quartz. *The Journal of Chemical Physics*, **69**, 4876–4884.

Isoya J., Weil J.A. and Davis P.H. (1983) EPR of atomic-hydrogen ^{1}H and ^{2}H in α-quartz. *Journal of Physics and Chemistry of Solids,* **44**, 335–343.

Isoya J., Tennant W.C. and Weil J.A. (1988) Electron-paramagnetic-res of the TiO_4/Li center in crystalline quartz. *Journal of Magnetic Resonance,* **79**, 90–98.

Jacamon F. and Larsen R. (2009) Trace element evolution of quartz in the charnockitic Kleivan granite, SW-Norway: the Ge/Ti ratio of quartz as an index of igneous differentiation. *Lithos*, **107**, 281–291.

Jaeger D., Stalder R., Masago H. and Strasser M. (2019) OH defects in quartz as a provenance tool: application to fluvial and deep marine sediments from SW Japan. *Sedimentary Geology*, **388**, 66–80.

Jani M.G., Bossoli R.B. and Halliburton L.E. (1983) Further characterization of the E'_1 center in crystalline SiO_2. *Physical Reviews B*, **27**, 2285–2293.

Jollands M.C., Blanchard M. and Balan E. (2020) Structure and theoretical infrared spectra of OH defects in quartz. *European Journal of Mineralogy*, **32**, 311–323.

Jones C.E. and Embree D. (1976) Correlations of the 4.77–4.28 eV luminescence band in silicon dioxide with oxygen vacancy. *Journal of Applied Physics*, **47**, 5365–5371.

Jourdan A.-L., Vennemann T.W., Mullis J., Ramseyer K. and Spiers C.J. (2009) Evidence of growth and sector zoning in hydrothermal quartz from Alpine veins. *European Journal Mineralogy*, **21**, 219–231.

Kats A. (1962) Hydrogen in alpha quartz. *Philips Research Reports*, **17**, 133–279.

Kelly J.L., Fu B., Kita N.T., Valley J.W. (2007) Optically continuous silcrete quartz cements of the St. Peter sandstone: High precision oxygen isotope analysis by ion microprobe. *Geochimica et Cosmochimica Acta*, **71**, 3812–3832.

Kempe U., Götze J., Dandar S. and Habermann D. (1999) Magmatic and metasomatic processes during formation of the Nb-Zr-REE deposits from Khaldzan Buregte (Mongolian Altai): indications from a combined CL-SEM study. *Mineralogical Magazine*, **63**, 165–167.

Kempe U., Götze J., Enchbat D., Monecke T. and Poutivtsev M. (2012) Quartz regeneration and its use as a repository of genetic information. Pp. 331–355 in: *Quartz: Deposits, Mineralogy and Analytics*. (J. Götze and R. Möckel, editors). Springer Geology, Heidelberg-New York-Dordrecht-London.

Kihara K. (1990) An X-ray study of the temperature dependence of the quartz structure. *European Journal of Mineralogy*, **2**, 63–77.

Komur, K., Horikawa Y. and Toyoda S. (2002) Development of radiation-damage halos in low-quartz: cathodoluminescence measurement after He^{+} ion implantation. *Mineralogy and Petrology*, **76**, 261–266.

Krickl R., Nasdala L., Götze J., Grambole D. and Wirth R. (2008) Alteration of SiO_2 caused by natural and artificial alpha-irradiation. *European Journal of Mineralogy*, **20**, 517–522.

Ladenburger S., Walter B.F., Marks M.A.W. and Markl G. (2020) Combining ion chromatography and total reflection X-ray fluorescence for detection of major, minor and trace elements in quartz-hosted fluid inclusions. *Journal of Analytical Chemistry*, **75**, 1477–1485.

Laman F.C. and Weil J.A. (1977) Silver-compensated germanium center in α-quartz. *Journal of Physics and Chemistry of Solids*, **38**, 949–956.

Laman F.C. and Weil J.A. (1978) A germanium tri-hytrogen center in alpha-quartz. Pp. 253–257 in: *The Physics of SiO_2 and its interfaces* (S.T. Pantelides, editor). Pergamon, New York, USA.

Lan Q., Lin J., Fu S. and Luo J. (2021) Cathodoluminescent textures and trace element signatures of hydrothermal quartz from the granite-related No. 302 uranium deposit, South China: A reconnaissance study for their genetic significances. *Journal of Geochemical Exploration*, **224**, 106740. doi.org/10.1016/j.gexplo.2021.106740.

Landtwing M. and Pettke T. (2005) Relationships between SEM-cathodoluminescence response and trace-element composition of hydrothermal vein quartz. *American Mineralogist*, **90**, 122–131.

Larsen R.B., Polvé M. and Juve G. (2000) Granite pegmatite quartz from Evje-Iveland: trace-element chemistry and implications for the formation of high-purity quartz. *NGU Bulletin*, **436**, 57–59.

Larsen R.B., Henderson I., Ihlen P.M. and Jacamon F. (2004) Distribution and petrogenetic behaviour of trace elements in granitic pegmatite quartz from South Norway. *Contributions Mineralogy Petrology*, **147**, 615–628.

Leeman W.P., McRae C.M., Wilson N.C., Torpy A., Lee C.-T.A., Student J.J., Thomas J.B. and Vicenzi E.P. (2012) A study of cathodoluminescence and trace element compositional zoning in natural quartz from volcanic rocks: Mapping titanium content in quartz. *Microscopy and Microanalysis*, **18**, 1322–1341.

Lees N.S., Walsby C.J., Williams J.A.S., Weil J.A. and Claridge R.F.C. (2003) EPR of a hydrogen/double-lithium centre in α-quartz. *Physics and Chemistry of Minerals*, **30**, 131–141.

https://doi.org/10.1180/mgm.2021.72 Published online by Cambridge University Press

Lehmann G. (1978) Farbe von Mineralien und ihre Ursachen. *Fortschritte Mineralogie*, **56**/2, 172–252.

Lehmann G. and Bambauer H.U. (1973) Quarzkristalle und ihre Farben. *Angewandte Chemie*, **85**, 281–289.

Lehmann G. and Moore W.I. (1966) Optical and paramagnetic properties of iron centers in quartz. *Journal of Chemical Physics*, **44**, 1741–1745.

Lehmann K., Pettke T. and Ramseyer K. (2011) Significance of trace elements in syntaxial quartz cement, Haushi Group sandstones, Sultanate of Oman. *Chemical Geology*, **280**, 47–57.

Le Page Y., Calvert L.D. and Gabe E.J. (1980) Parameter variation in low-quartz between 94 and 298 K. *Journal of Physics and Chemistry of Solids*, **41**, 721–725.

Li Z. and Pan Y. (2012) First-principles calculations of the E'_1 center in quartz: structural models, ^{29}Si hyperfine parameters and association with Al impurity. Pp. 161–175 in: *Quartz: Deposits, Mineralogy and Analytics*. (J. Götze and R. Möckel, editors). Springer Geology, Heidelberg-New York-Dordrecht-London.

Li J., Hu R., Xiao J., Zhuo Y., Yan J. and Oyebamiji A. (2020) Genesis of gold and antimony deposits in the Youjiang metallogenic province, SW China: Evidence from in situ oxygen isotopic and trace element compositions of quartz. *Ore Geology Reviews*, **116**, 103257.

Lin J.S., Payne M.C., Heine V. and McConnell J.D.C. (1994) Ab initio calculations on $(OH)_4$ defects in α-quartz. *Physics and Chemistry of Minerals*, **21**, 150–155.

Lipin B.R. and McKay G.A. (Editors)(1986) *Geochemistry and Mineralogy of Rare Earth Elements*. Reviews in Mineralogy, **21**. The Mineralogical Society of America, Washington DC, 349 pp.

Luff B.J. and Townsend P.D. (1990) Cathodoluminescence of synthetic quartz. *Journal Physics Condensed Matter*, **2**, 8089–8097.

Luo K., Zhou J.-X., Huang Z.-L., Caulfield J., Zhao J.-X., Feng Y.-X. and Ouyang H. (2020) New insights into the evolution of Mississippi-Valley-Type hydrothermal system: A case study of the Wusihe Pb-Zn deposit, south China, using quartz in-situ trace elements and sulfides in-situ S-Pb isotopes. *American Mineralogist*, **105**, 35–51.

Ma C., Goreva J.S. and Rossman G.R. (2002) Fibrous nanoinclusions in massive rose quartz: HRTEM and AEM investigations. *American Mineralogist*, **87**, 269–276.

Mackey J.H. (1963) EPR study of impurity-related color centers in germanium-doped quartz. *Journal of Chemical Physics*, **39**, 74–83.

Mackey J.H., Boss J.W. and Wood D.E. (1970) EPR study of substitutional-aluminum-related hole centers in synthetic α-quartz. *Journal of Magnetic Resonance*, **3**, 44–54.

Mao W., Rusk B., Yang F. and Zhang M. (2017) Physical and chemical evolution of the Dabaoshan Porphyry Mo deposit, South China: Insights from fluid inclusions, cathodoluminescence, and trace elements in quartz. *Economic Geology*, **112**, 889–918.

Maschmeyer D. and Lehmann G. (1983) A trapped-hole center causing rose coloration of natural quartz. *Zeitschrift für Kristallographie*, **163**, 181–196.

Mashkovtsev R.I. and Pan Y. (2011) Biradical states of oxygen-vacancy defects in alpha-quartz: centers E''_2 and E''_4. *Physics and Chemistry of Minerals*, **38**, 647–54.

Mashkovtsev R.I. and Pan Y. (2012a) Five new E' centers and their ^{29}Si hyperfine structure in electron-irradiated α-quartz. *Physics and Chemistry of Minerals*, **39**, 79–85.

Mashkovtsev R.I. and Pan Y. (2012b) Stable states of E'' defects in α-quartz. *EPL*, **98**, 56005.

Mashkovtsev R.I. and Pan Y. (2013) Nature of paramagnetic defects in α-quartz: Progresses in the First Decade of the 21st Century. Pp. 65–104 in: *New Developments in Quartz Research: Varieties, Crystal Chemistry and Uses in Technology* (B. Novak and P. Marek, editors). Nova Science Publishers, New York, USA.

Mashkovtsev R.I. and Pan Y. (2014) Triplet states of oxygen-vacancy defects in α-quartz: Center E''_9. *EPL*, **107**, 36005.

Mashkovtsev R.I. and Pan Y. (2016) New E' centers in neutron-irradiated α-quartz. *EPL*, **113**, 64004.

Mashkovtsev R.I. and Pan Y. (2018) EPR study of new E^{κ} centers in neutron-irradiated α-quartz. *EPL*, **124**, 54001.

Mashkovtsev R.I., Shcherbakova M.Ya. and Solntsev V.P. (1978) EPR of radiation hole centers in α-quartz. *Trudy Instituta Geologii i Geofyziki Akademii Nauk SSSR, Sib. Otd.*, **385**, 78–86 [in Russian].

Mashkovtsev R.I., Howarth D.H. and Weil J.A. (2007) Biradical states of oxygen-vacancy defects in α-quartz. *Physical Reviews B*, **76**, 214114.

Mashkovtsev R.I., Li Z., Mao M. and Pan Y. (2013) ^{73}Ge, ^{17}O and ^{29}Si hyperfine interactions of the Ge E'_1 center in crystalline SiO_2. *Journal of Magnetic Resonance*, **233**, 7–16.

Mashkovtsev R.I., Botis S.M., Nilges M.J. and Pan Y. (2019) Paramagnetic defects in neutron-irradiated α-quartz: Novel Al-associated E' centers. *EPL*, **128**, 54004.

Matyash I.V., Brik A.B., Zayats A.P. and Masykin V.V. (1987) *Radiospectroscopy of Quartz*. Naukova Dumka, Kiev, USSR.

McBride E.F. (1989) Quartz cement in sandstones: a review. *Earth Science Reviews*, 26, 69–112.

McCandless T.E., Lajack D.J., Ruiz J. and Ghazi A.M. (1997) Trace element determination of single fluid inclusions in quartz by Laser Ablation ICP-MS. *Geostandard Newsletter*, **21**, 279–287.

McConnell J.D.C., Lin J.S. and Heine V. (1995) The solubility of $[4H]_{Si}$ defects in α-quartz and their role in the formation of molecular water and related weakening on heating. *Physics and Chemistry of Minerals*, **22**, 357–366.

McEachern R.J. and Weil J.A. (1994) ^{17}O hyperfine interaction for the $[GeO_4]^-_{I, II}$ and $[GeO_4/Li]^0_{A,C}$ centers in an enriched crystal of alpha-quartz. *Physical Review B*, **49**, 6698–6709.

McEachern R.J., Weil J.A. and Sawyer B. (1992) Distortion and ^{17}O hyperfine interaction in the centres $[GeO_4]_{I,II}$ in α-quartz. *Solid State Communications*, **81**, 207–209.

McLaren A.C., Cook R.F., Hyde S.T. and Tobin R.C. (1983) The mechanisms of the formation and growth of water bubbles and associated dislocation loops in synthetic quartz. *Physics and Chemistry of Minerals*, **9**, 79–94.

McLaren A.C., Fitz Gerald J.D. and Gerretsen J. (1989) Dislocation nucleation and multiplication in synthetic quartz: relevance to water weakening. *Physics and Chemistry of Minerals*, **16**, 465–482.

Meunier J.D., Sellier E. and Pagel M. (1990) Radiation-damage rims in quartz from uranium-bearing sandstones. *Journal of Sedimentary Petrology*, **60**, 53–58.

Meyer B.K., Lohse F., Spaeth J.M. and Weil J.A. (1984) Optically detected magnetic resonance of the $[AlO_4]^0$ centre in crystalline quartz. *Journal of Physics C: Solid State Physics*, **17**, L31–L36.

Mineeva R.M., Bershov L.V. and Petrov I. (1991) EPR of surficially bound Fe^{3+} ions in polycrystalline quartz. *Doklady Akademii Nauk SSSR*, **321**/2, 368–372 [in Russian].

Minge, J. Weil J.A. and McGavin D.G. (1989) EPR study of Fe^{3+} in alpha-quartz – characterization of a new type of cation-compensated center. *Physical Review B*, **40**, 6490–6498.

Minge J., Mombourquette M.J. and Weil J.A. (1990) EPR study of Fe^{3+} in alpha-quartz – the sodium-compensated center. *Physical Review B*, **42**, 33–36.

Miyoshi N., Yamaguchi Y. and Makino K. (2005) Successive zoning of Al and H in hydrothermal vein quartz. *American Mineralogist*, **90**, 310–315.

Moiseev B.M. (1985) *Radiation Processes in Minerals*. Nedra, Moscow, Russia [in Russian].

Mombourqette M.J., Tennant W.C. and Weil J.A. (1986) EPR study of Fe^{3+} in alpha-quartz – a reexamination of the so-called I-center. *Journal of Chemical Physics*, **85**, 68–79.

Mombourqette M.J., Minge I., Hantehzadeh M.R., Weil J.A. and Halliburton L.E. (1989) EPR study of Fe^{3+} in alpha-quartz: Hydrogen-compensated center. *Physical Review B*, **39**, 4004–4008.

Monecke T., Kempe U., Petersen S., Götze J., Herzig P. and Wolf D. (1999) Trace element characteristics of quartz from the TAG hydrothermal mound. Pp. 551–554 in: *Mineral Deposits: Processes to Processing* (C.J. Stanley *et al.*, editors). Balkema, Rotterdam, Netherlands.

Monecke T., Bombach G., Klemm W., Kempe U., Götze J. and Wolf D. (2000) Determination of trace elements in quartz standard UNS-SpS and in natural quartz by ICP-MS. *Geostandards Newsletter*, **24**/1, 73–81.

Monecke T., Kempe U. and Götze J. (2002) Genetic significance of the trace element content in metamorphic and hydrothermal quartz: A reconnaissance study. *Earth and Planetary Science Letters*, **202**, 709–724.

https://doi.org/10.1180/mgm.2021.72 Published online by Cambridge University Press

Monecke T., Dulski P. and Kempe U. (2007) Origin of convex tetrads in rare earth element patterns of hydrothermally altered siliceous igneous rocks from the Zinnwald Sn-W deposit, Germany. *Geochimica et Cosmochimica Acta*, **71**, 335–353.

Monnier L., Lach P., Salvi S., Melleton J., Bailly L., Béziat D., Monnier Y. and Gouy S. (2018) Quartz trace-element composition by LA-ICP-MS as proxy for granite differentiation, hydrothermal episodes, and related mineralization: The Beauvoir Granite (Echassières district), France. *Lithos*, **320**, 355–377.

Monnier L., Salvi S., Pochon A., Melleton J., Béziat D., Lach P. and Bailly L. (2021) Antimony in quartz as a vector to mineralization: A statistical approach from five Variscan Sb occurrences (France). *Journal of Geochemical Exploration*, **221**, 106705.

Müller A. and Knies J. (2013) Trace elements and cathodoluminescence of detrital quartz in Arctic marine sediments – a new ice-rafted debris provenance proxy. *Climate Past*, **9**, 2615–2630.

Müller A. and Koch-Müller M. (2009) Hydrogen speciation and trace element contents of igneous, hydrothermal and metamorphic quartz from Norway. *Mineralogical Magazine*, **73**, 569–584.

Müller A., Kronz A. and Breiter K. (2002) Trace elements and growth patterns in quartz: a fingerprint of the evolution of the subvolcanic Podlesi granite system (Krušné Hory, Czech Republic). *Bulletin of the Czech Geological Survey*, **77**, 135–145.

Müller A., Wiedenbeck M., Van den Kerkhof A.M., Kronz A. and Simon K. (2003) Trace elements in quartz – a combined electron microprobe, secondary ion mass spectrometry, laser-ablation ICP-MS, and cathodoluminescence study. *European Journal of Mineralogy*, **15**, 747–763.

Müller A., Breiter K., Seltmann R. and Pécskay Z. (2005) Quartz and feldspar zoning in the eastern Erzgebirge volcano-plutonic complex (Germany, Czech Republic): evidence of multiple magma mixing. *Lithos*, **80**, 201–227.

Müller A., Ihlen P.M. and Wanvik J.E. (2007) High-purity quartz mineralisation in kyanite quartzites, Norway. *Mineralium Deposita*, **42**, 523–535.

Müller A., Wiedenbeck M., Flem B. and Schiellerup H. (2008) Refinement of phosphorus determination in quartz by LA-ICP-MS through new reference material values. *Geostandards and Geoanalytical Research*, **32**, 361–376.

Müller A., Herrington R., Armstrong R., Seltmann R., Kirwin D.J., Stenina N.G. and Kronz A. (2010) Trace elements and cathodoluminescence of quartz in stockwork veins of Mongolian porphyry-style deposits. *Mineralium Deposita*, **45**, 707–727.

Müller A., Wanvik J.E. and Ihlen P.M. (2012) Petrological and chemical characterisation of high-purity quartz deposits with examples from Norway. Pp. 71–118 in: *Quartz: Deposits, Mineralogy and Analytics*. (J. Götze and R. Möckel, editors). Springer Geology, Heidelberg-New York-Dordrecht-London.

Müller A., Ihlen P.M., Snook B., Larsen R.B., Flem B., Bingen B. and Williamson B.J. (2015) The chemistry of quartz in granitic pegmatites of Southern Norway: Petrogenetic and economic implications. *Economic Geology*, **110**, 1737–1757.

Müller A., Romer R.L. and Pedersen R.-B. (2017) The Sveconorwegian pegmatite province – Thousands of pegmatites without parental granites. *The Canadian Mineralogist*, **55**, 283–315.

Müller A., Herklotz G. and Giegling H. (2018) Chemistry of quartz related to the Zinnwald/Cínovec Sn-W-Li greisen-type deposit, Eastern Erzgebirge, Germany. *Journal of Geochemical Exploration*, **190**, 357–373.

Müller A., Keyser W., Simmons W.B., Webber K., Wise M., Beurlen H., Garate-Olave I., Roda-Robles E. and Galliski M.A. (2021) Quartz chemistry of granitic pegmatites: Implications for classification, genesis and exploration. *Chemical Geology*, https://doi.org/10.1016/j.chemgeo.2021.120507.

Nilges M.J., Pan Y. and Mashkovtsev R.I. (2008) Radiation-induced defects in quartz. I. Single-crystal W-band EPR study of an electron irradiated quartz. *Physics and Chemistry of Minerals*, **35**, 103–115.

Nilges M.J., Pan Y. and Mashkovtsev R.I. (2009) Radiation-induced defects in quartz. III. EPR, ENDOR and ESEEM characterization of a peroxy radical. *Physics and Chemistry of Minerals*, **36**, 63–71.

Nuttall R.H.D. and Weil J.A. (1980) Two hydrogenic trapped-hole species in α-quartz. *Solid State Communications*, **33**, 99–102.

Nuttall R.H.D. and Weil J.A. (1981a) The magnetic properties of the oxygen-hole aluminum centers in crystalline SiO_2. I. $[AlO_4]^0$. *Canadian Journal of Physics*, **59**, 1886–1892.

Nuttall R.H.D. and Weil J.A. (1981b) The magnetic properties of the oxygen-hole aluminum centers in crystalline SiO_2. II. $[AlO_4/H^+]^+$ and $[AlO_4/Li^+]^+$. *Canadian Journal of Physics*, **59**, 1709–1718.

Nuttall R.H.D. and Weil J.A. (1981c) The magnetic properties of the oxygen-hole aluminum centers in crystalline SiO_2. III. $[AlO_4]^+$. *Canadian Journal of Physics*, **59**, 1886–1892.

O'Brien M.C.M. (1955) The structure of the colour centres in smoky quartz. *Proceedings of the Royal Society*, **A231**, 404–414.

Owen M.R. (1988) Radiation-damage halos in quartz. *Geology*, **16**, 529–532.

Pacák K., Zacharias J. and Strnad L. (2019) Trace-element chemistry of barren and ore-bearing quartz of selected Au, Au-Ag and Sb-Au deposits from the Bohemian Massif. *Journal of Geosciences*, **64**, 19–35.

Pan Y. and Nilges M.J. (2014) Electron paramagnetic resonance (EPR) spectroscopy: Basic principles, experimental techniques and applications to Earth and planetary sciences. Pp. 655–690 in: *Spectroscopic Methods in Mineralogy and Material Sciences* (G.S. Henderson, D.R. Neuville and R.T. Downs, editors). Reviews in Mineralogy and Geochemistry, Volume 78. The Mineralogical Society of America and the Geochemical Society, Chantilly, Virginia, USA.

Pan Y., Botis S. and Nokhrin S. (2006) Applications of natural radiation-induced paramagnetic defects in quartz to exploration in sedimentary basins. *Journal of China University of Geosciences*, **17**, 258–271.

Pan Y., Nilges M.J. and Mashkovtsev R.I. (2008) Radiation-induced defects in quartz. II. W-band single-crystal EPR study of natural citrine. *Physics and Chemistry of Minerals*, **35**, 387–397.

Pan Y., Nilges M.J. and Mashkovtsev R.I. (2009) Radiation-induced defects in quartz: a multifrequency EPR study and DFT modelling of new peroxy radicals. *Mineralogical Magazine*, **73**, 519–536.

Pan Y., Li D., Feng R., Wiens E., Chen N., Götze J. and Lin J. (2021) Uranyl binding mechanism in microcrystalline silicas: A potential missing link for uranium mineralization by direct uranyl co-precipitation and environmental implications. *Geochimica et Cosmochimica Acta*, **292**, 518–531.

Perlson B.D. and Weil J.A. (2008) Electron paramagnetic resonance studies of the E' centers in alpha-quartz. *Canadian Journal of Physics*, **86**, 871–881.

Perny B., Eberhardt P., Ramseyer K. and Mullis J. (1992) Microdistribution of aluminium, lithium and sodium in quartz: Possible causes and correlation with short-lived cathodoluminescence. *American Mineralogist*, **77**, 534–544.

Peterková T. and Dolejš J. (2019) Magmatic-hydrothermal transition of Mo-W-mineralized granite-pegmatite-greisen system recorded by trace elements in quartz: Krupka district, Eastern Krušné hory/Erzgebirge. *Chemical Geology*, **523**, 179–202.

Plötze M. and Wolf D. (1996) EPR- and TL-spectra of quartz: Irradiation dependence of $[TiO_4/Li^+]^-$ centres. *European Journal of Mineralogy*, **8**, 217 [in German].

Potrafke A., Stalder R., Schmidt B.C. and Ludwig T. (2019) OH defect contents in quartz in a granitic system at 1–5 kbar. *Contributions to Mineralogy and Petrology*, **174**, 98.

Potrafke A., Breiter K., Ludwig T., Neuser R.D. and Stalder R. (2020) Variations of OH defects and chemical impurities in quartz within igneous bodies. *Physics and Chemistry of Minerals*, **47**, 24.

Pott G.T. and McNicol B.D. (1971) Spectroscopic study of the coordination and valence of Fe and Mn ions in and on the surface of aluminas and silicas. *Discussion Faraday Society*, **52**, 121–131.

Rakov L.T., Milovidova N.D., Kuvshinova K.A. and Moiseev B.M. (1985) Investigation of Ge-centres in natural polycrystalline quartz using EPR. *Geokhimiya*, **9**, 1339–1344 [in Russian].

Ramseyer K. and Mullis J. (1990) Factors influencing short-lived blue cathodoluminescence of alpha-quartz. *American Mineralogist*, **75**, 791–800.

Ramseyer K., Baumann J., Matter A. and Mullis J. (1988) Cathodoluminescence colours of alpha-quartz. *Mineralogical Magazine*, **52**, 669–677.

Remond G., Cesbron F., Chapoulie R., Ohnenstetter D., Roques-Carmes C. and Schvoerer M. (1992) Cathodoluminescence applied to the microcharacterization of mineral materials: a present status in experimentation and interpretation. *Scanning Microscopy*, **6**, 23–68.

Richter D.K. (1971) Fazies- und Diagenesehinweise durch Einschlüsse in authigenen Quarzen. *Neues Jahrbuch Geologie Paläonthologie, Monatshefte*, **10**, 604–622.

https://doi.org/10.1180/mgm.2021.72 Published online by Cambridge University Press

Rink W.J., Rendell H., Marseglia E.A., Luff B.J. and Townsend P.D. (1993) Thermoluminescence spectra of igneous quartz and hydrothermal vein quartz. *Physics and Chemistry of Minerals,* **20**, 353–361.

Rinneberg H. and Weil J.A. (1972) EPR Studies of Ti^{3+}-H^{+} centers in X-irradiated alpha-quartz. *Journal of Chemical Physics*, **56**, 2019–2028.

Rossman G.R. (1994) Colored varieties of the silica minerals. Pp. 433–467 in: *Silica: Physical Behavior, Geochemistry, and Materials Applications* (P.J. Heaney, C.T. Prewitt, and G.V. Gibbs, editors). Reviews in Mineralogy, **Vol. 29**. Mineralogical Society of America, Washington DC.

Rossman G.R., Weis D. and Wasserburg G.J. (1987) Rb, Sr and Sm concentrations in quartz. *Geochimica et Cosmochimica Acta*, **51**, 2325–2329.

Rusk B. (2012) Cathodoluminescent textures and trace elements in hydrothermal quartz. Pp. 307–330 in: *Quartz: Deposits, Mineralogy and Analytics*. (J. Götze and R. Möckel, editors). Springer Geology, Heidelberg-New York-Dordrecht-London.

Rusk B., Reed M.H., Dilles J.H. and Kent A.J.R. (2006) Intensity of quartz cathodoluminescence and trace-element content in quartz from the porphyry copper deposit at Butte, Montana. *American Mineralogist,* **91**, 1300–1312.

Rusk B., Lowers H.A. and Reed M.H. (2008) Trace elements in hydrothermal quartz: Relationships to cathodoluminescent textures and insights into vein formation. *Geology,* **36**, 547–550.

Rusk B., Koenig A. and Lowers H. (2011) Visualizing trace element distribution in quartz using cathodoluminescence, electron microprobe, and laser ablation-inductively coupled plasma-mass spectrometry. *American Mineralogist*, **96**, 703–708.

Scala C.M. and Hutton D.R. (1976) Site assignement of Fe^{3+} in alpha-quartz. *Physics status solidi b*, **73**, K115–K117.

Schofield P.F., Henderson C.M.B., Cressey G. and Van der Laan G. (1995) 2p X-ray absorption spectroscopy in the earth sciences. *Journal of Synchrotron Radiation*, **2**, 93–98.

Scholz R., Chaves M.L.S.C., Krambrock K., Pinheiro M.V.B., Barreto S.B. and De Menezes M.G. (2012) Brazilian quartz deposits with special emphasis on gemstone quartz and its color treatment. Pp. 139–159 in: *Quartz: Deposits, Mineralogy and Analytics*. (J. Götze and R. Möckel, editors). Springer Geology, Heidelberg-New York-Dordrecht-London.

Schrön, W., Baumann L. and Rank K. (1982) Zur Charakterisierung von Quarzgenerationen in den postmagmatogenen Erzformationen des Erzgebirges. *Zeitschrift für Geologische Wissenschaften*, **10**, 1499–1521.

Schrön W., Schmädicke E., Thomas R. and Schmidt W. (1988) Geochemische Untersuchungen an Pegmatitquarzen. *Zeitschrift für Geologische Wissenschaften*, **16**, 229–244.

Seifert W., Rhede D., Thomas R., Förster H.-J., Lucassen F., Dulski P. and Wirth R. (2011) On the origin of igneous blue quartz: inferences from a multi-analytical study of submicron mineral inclusions. *Mineralogical Magazine*, **75**, 2519–2534.

Siegel G.H. and Marrone M.J. (1981) Photoluminescence in as-drawn and irradiated silica optical fibers: An assessment of the role of nonbridging oxygen defect centres. *Journal of Non-Crystalline Solids,* **45**, 235–247.

Sittner J. (2019) *Untersuchungen zur Spurenelementgeochemie von Pegmatitquarzen aus der Region Tørdal, Norwegen mittels LA-ICP-MS, SIMS und Kathodolumineszenz*. Master thesis, TU Bergakademie Freiberg, Germany.

Sittner J. and Götze J. (2018) Cathodoluminescence (CL) characteristics of quartz from different metamorphic rocks within the Kaoko belt (Namibia). *Minerals*, **8**, 190.

SivaRamaiah G. and Pan Y. (2012) Thermodynamic properties and magnetic susceptibility of surface Fe^{3+} species on quartz: Effects of gamma ray irradiation and implications for aerosol-radiation interactions. *Physics and Chemistry of Minerals*, **39**, 515–523.

SivaRamaiah G., Lin J. and Pan Y. (2011) Electron paramagnetic resonance spectroscopy of Fe^{3+} ions in amethyst: Thermodynamic potentials and magnetic susceptibility. *Physics and Chemistry of Minerals*, **38**, 159–167.

Skuja L. (1998) Optically active oxygen-deficiency-related centers in amorphous silicon dioxid. *Journal of Non-Crystalline Solids*, **239**, 16–48.

Smith G., Vance E.R., Hasan Z., Edgar A. and Runciman W.A. (1978) A charge transfer mechanism for the colour of rose quartz. *Physica status solidi a*, **46**, K135–K140.

Soong R. and Blattner P. (1986) Biterminal authigenic ^{18}O-enriched quartz in a subbituminous coal seam, Charleston, New Zealand. *New Zealand Journal of Geology and Geophysics*, **29**, 141–145.

Stalder R. (2021) OH point defects in quartz – a review. *European Journal of Mineralogy*, **33**, 145–163.

Stalder R., Potrafke A., Billström K., Skogby H., Meinhold G., Gögele C. and Berberich T. (2017) OH defects in quartz as monitor for igneous, metamorphic, and sedimentary processes. *American Mineralogist*, **102**, 1832–1842.

Stalder R., von Eynatten H., Costamoling J., Potrafke A., Dunkl I. and Meinhold G. (2019) OH in detrital quartz grains as tool for provenance analysis: Case studies on various settings from Cambrian to Recent. *Sedimentary Geology*, **389**, 121–126.

Stegger P. and Lehmann G. (1989) The structures of three centers of trivalent iron in alpha-quartz. *Physics and Chemistry of Minerals*, **16**, 401–407.

Stenina N.G. (2004) Water-related defects in quartz. *Bulletin of Geosciences*, **79**, 251–268.

Stevens-Kalceff M.A. (2009) Cathodoluminescence microcharacterization of point defects in α-quartz. *Mineralogical Magazine*, **73**, 585–606.

Stevens-Kalceff M.A. and Phillips M.R. (1995) Cathodoluminescence microcharacterization of the defect structure of quartz. *Physical Reviews B*, **52**, 3122–3134.

Stevens-Kalceff M.A., Phillips M.R., Moon A.R. and Kalceff W. (2000) Cathodoluminescence microcharacterization of silicon dioxide polymorphs. Pp. 193–224 in: *Cathodoluminescence in Geosciences* (M. Pagel, V. Barbin, P. Blanc, and D. Ohnenstetter, editors). Springer, Berlin Heidelberg New York Tokyo.

Tollan P., Ellis B., Troch J. and Neukampf J. (2019) Assessing magmatic volatile equilibria through FTIR spectroscopy of unexposed melt inclusions and their host quartz: a new technique and application to the Mesa Falls Tuff, Yellowstone. *Contributions to Mineralogy and Petrology*, **174**, 24.

Toyoda S. (2011) The E'_1 center in natural quartz: its formation and applications to dating and provenance researches. *Geochronometria*, **38**, 242–248.

Toyoda S. (2016) ESR signals in quartz: Applications to provenance research – A review. *Quaternary International*, **397**, 258–266.

Van den Kerkhof A.M., Kronz A., Simon K. and Scherer T. (2004) Fluid-controlled quartz recovery in granulite as revealed by cathodoluminescence and trace element analysis (Bamble sector, Norway). *Contributions to Mineralogy and Petrology*, **146**, 637–652.

Walenczak Z. (1969) Geochemistry of minor elements dispersed in quartz (Ge, Al, Ga, Fe, Ti, Li and Be). *Archivum Mineralogizne*, **28**, 189–335 [in Polish].

Walker G. (1985) Mineralogical applications of luminescence techniques. Pp. 103–140 in: *Chemical Bonding and Spectroscopy in Mineral Chemistry* (F.J. Berry and D.J. Vaughan, editors). Chapman and Hall, London, Great Britain.

Walsby C.J., Less N.S., Claridge R.F.C. and Weil J.A. (2003) The magnetic properties of oxygen-hole aluminum centers in crystalline SiO_2. VI. A stable AlO_4/Li centre. *Canadian Journal of Physics*, **81**, 583–598.

Wang D., Liu J., Carranza E.J.M., Zhai D., Wang Y., Zhen S., Wang J., Wang J., Liu Z. and Zhang F. (2019) Formation and evolution of snowball quartz phenocrysts in the Dongping porphyritic granite, Hebei province, China: Insights from fluid inclusions, cathodoluminescence, trace elements, and crystal size distribution study. *Lithos*, 340–341, 239–254.

Wark D.A. and Watson E.B. (2006) TitaniQ: a titanium-in-quartz geothermometer. *Contributions to Mineralogy and Petrology*, **152**, 743–754.

Watt G.R., Wright P., Galloway S. and McLean C. (1997) Cathodoluminescence and trace element zoning in quartz phenocrysts and xenocrysts. *Geochimica et Cosmochimica Acta*, **61**, 4337–4348.

Weil J.A. (1971) Germanium-hydrogen-lithium-center in quartz. *Journal of Chemical Physics*, **55**, 4685–4698.

Weil J.A. (1984) A review of electron spin spectroscopy and its application to the study of paramagnetic defects in crystalline quartz. *Physics and Chemistry of Minerals*, **10**, 149–165.

Weil J.A. (1993) A review of the EPR spectroscopy of the point defects in α-quartz: The decade 1982–1992. Pp. 131–144 in: *Physics and Chemistry*

https://doi.org/10.1180/mgm.2021.72 Published online by Cambridge University Press

of SiO_2 and the Si-SiO Interface 2 (C.R. Helms and B.E. Deal, editors). Plenum Press, New York, USA.

Weil J.A. (1994) EPR of iron centres in silicon dioxide. *Applied Magnetic Resonance*, **6**, 1–16.

Wertich V., Leichmann J., Dosbaba M. and Götze J. (2018) Multi-stage evolution of gold-bearing hydrothermal quartz veins at the Mokrsko gold deposit (Czech Republic) based on cathodoluminescence, spectroscopic, and trace elements analyses. *Minerals*, **8**, 335.

Wood S.A. (1990) The aqueous geochemistry of the rare-earth elements and yttrium. 2. Theoretical predictions of speciation in hydrothermal solutions to 350 °C at saturation water vapor pressure. *Chemical Geology*, **88**, 99–125.

Wright P.M., Weil J.A., Buch T. and Anderson J.H. (1963) Titanium colour centers in rose quartz. *Nature*, **197**, 246–248.

Yang X.H. and McKeever S.W.S. (1990) Point defects and predose effect in quartz. *Radiation Protection Dosimetry*, **33**, 27–30.

Yang L., Mashkovtsev R., Botis S. and Pan Y. (2007) Multi-spectroscopic study of green quartzite (Guizhou Jade) from the Qinglong antimony deposit, Guizhou Province, China. *Journal of China University of Geosciences*, **18**, 383–386.

Zolensky M.E., Sylvester P.J. and Paces J.B. (1988) Origin and significance of blue coloration in quartz from Llano rhyolite (llanite), north-central Llano county, Texas. *American Mineralogist*, **73**, 313–332.

https://doi.org/10.1180/mgm.2021.72 Published online by Cambridge University Press